Abstract

Title of Document	Application of Plate Heat Exchanger for Low Temperature Lift Heat Pump Systems
	Song Li, Master of Science, 2012
Advisor	Professor Reinhard Radermacher, Department of Mechanical Engineering

In this thesis I investigated the energy saving potential of a low temperature lift heat pump (LTLHP) such as water source heat pump (WSHP), and studied the utilization of a plate heat exchanger (PHE) as the LTLHP evaporator. Due to the facility limitation, I only tested and studied the evaporator for LTLHP. Since the LTLHP requires a large water flow rate, its heat source liquid-to-refrigerant PHE is operated at lower refrigerant mass flux than typical applications. I varied the vapor quality, heat flux, evaporation pressure, and refrigerant mass flux to provide unique heat transfer characteristics, and I studied their effects on evaporation heat transfer. Based on the collected data, I concluded that at a low mass flux range, evaporation heat transfer is dominated by nucleate boiling, and convective boiling has mall influence. In addition, I carried out a simulation to compare the performance of WSHP with air source heat pump (ASHP).

Application of Plate Heat Exchanger for Low Temperature Lift Heat Pump Systems

By

Song Li

Thesis submitted to the Faculty of the Graduate School of the University of Maryland, College Park, in partial fulfillment of the requirement for the degree of Master of Science

2012

Advisor Committee:

Professor Reinhard Radermacher (Chair)

Associate Research Professor Yunho Hwang

Associate Professor Bao Yang

Table of Contents

List of Tables

List of Figures

Nomenclature

Symbols

A	Heat transfer area, m^2
A_x	Cross sectional flow area, m^2
b	Corrugation depth, m
β	Chevron angle, degree
C	Constant in equation
c_p	Specific heat, kJ/kg*K
d_e	Hydraulic diameter, m
ε	Energy balance, %
G	Mass flux, $kg/s*m^2$
ϒ	Channel aspect ratio, dimensionless
h	Enthalpy, kJ/kg or heat transfer coefficient, W/m^2*K
Δh	Enthalpy difference, kJ/kg
κ	Thermal conductivity, W/m*K
λ	Corrugation pitch, m
LMTD	Logarithmic mean temperature difference, K
L_p	Plate length, m
m	Slope of best fitting straight line
$\dot{m}$	Mass flow rate
n	Wilson plot method exponent
Nu	Nusselt number, dimensionless
ω	Uncertainty

P	Pressure or perimeter, kPa or m
p	Corrugation amplitude, m
Pr	Prandtl number, dimensionless
$\dot{Q}$	Heat transfer, W
q_w''	Heat flux based on warm water side, W/m^2
R	Thermal resistance, K/W
Re	Reynolds number, dimensionless
T	Temperature, ^oC
t	Plate thickness, m
ΔT	Temperature difference, K
ΔT_e	Excess temperature, ^oC
φ	Enlargement factor, dimensionless
U	Overall heat transfer coefficient, W/m^2*K
v	Velocity, m/s
w	Plate width, m
$\dot{W}$	Work, W
x	Quality, dimensionless

Acronyms

AACS	Air-cooled air-conditioning system
AC	Air-conditioning
ASHP	Air-source heat pump
ASHRAE	American Society of Heating Refrigeration and Air-Conditioning

	Engineers
BEC	Building Energy Consumption (kWh)
BPHE	Brazed plate heat exchanger
CFC	Chlorofluorocarbon
COP	Coefficient of performance
DHW	Domestic hot water
EIA	Energy Information Administration
EPA	Environmental Protection Agency
EXV	Electronic expansion valve
GCHP	Ground-coupled heat pump
GSHP	Ground-source heat pump
GWHP	Ground-water heat pump
GWP	Global Warming Potential
HCFC	Hydrochlorofluorocarbon
HFC	Hydrofluorocarbon
HTC	Heat transfer coefficient
HVAC	Heating, ventilation and air-conditioning
IEA	International Energy Agency
LMTD	Logarithmic mean temperature difference
LTLHP	Low temperature lift heat pump
MXV	Manual expansion valve
ODP	Ozone Depletion Potential
PHE	Plate heat exchanger

PID	Proportional-integral-derivative
PR	Pressure ratio
SWHP	Surface-water heat pump
TC	Thermocouple
VCC	Vapor compression cycle
USSHP	Urban sewage source heat pump
WACS	Water-cooled air-conditioning system
WSHP	Water-source heat pump
WWSHP	Waste water source heat pump
WWTP	Waste water treatment plant

Subscripts

avg	average
c	refrigerant side/cold water side
cond	condenser
evap	evaporator
i	in
m	mean
o	out
ov	overall
post	post-heating tape
pre	pre-heating tape
r	refrigerant

sat	saturation
t	pre-heating/post-heating tape
w	warm water side

Chapter 1. Introduction

1.1 Energy consumption overview

The world has been facing very serious energy crisis, due to its increasing energy consumption and depleting energy resources. As given by International Energy Agency (IEA) (2006), from 1984 to 2004, world-wide primary energy consumption increased by 49%, along with carbon dioxide emission increase of 43%, and the average annual growth was 2% and 1.8% respectively. For developed countries like the United States, total energy consumption was 9.36 trillion kWh in 1949, according to Energy Information Administration (EIA) (2011). Then in 2011, total consumption increased to 28.5 trillion kWh (EIA, 2011), more than tripled that in 62 years. Compared to developed countries, in emerging countries like China, the energy crisis is even more severe, due to their rising economy. For example, the energy consumption growth rate in China was 3.7%, between 1984 and 2004, and IEA estimates that it would only take 20 years for the country to double its energy consumption. In order to satisfy the fast rising energy demand, the use of high pollution energy sources is the typical solution, and by-products like carbon dioxide is directly emitted to the atmosphere. According to Yao et al. (2005), 75% of China's pollution originated from burning of coal as the primary energy source. Even though the United States is not known for serious air pollution, burning of coal still contributed to 28% of total energy production in 2011 (EIA, 2011).

1.1.1 Energy consumption in buildings

Among all energy uses, the building sector always takes up a significant portion. In developed countries like United Kingdom, building energy consumption was 39% of total energy use in 2004, which was more than that of industrial or transportation sector (Perez-Lombard et al., 2008). In a very dense urban environment such as New York City, building energy consumption even accounted for more than two thirds of the overall energy use (Inventory of New York City greenhouse emissions, 2010). Even though energy consumption percentage of building sector in developing country is lower than that in developed counties, it was forecasted to increase in the future. For instance, Chinese building sector accounted for 27.6% of total energy consumption in 2001 (Yao, 2005), and that number was expected to increase to 35% in 2020.

Based on an annual growth of more than 10% in building energy consumption (BEC) in China for the past twenty years, Cai et al. (2009) pointed out there were two major problems, namely low energy efficiency with huge energy waste in large-scale public buildings, and high BEC for heating in Northern China. Compared to Northern Europe with similar climate, insulation in China is very poor and efficiency of heating system is low, making the energy consumption for heating in China is about two to four times of that in Northern Europe. Space heating is also extending its applied region to more southern China provinces, and it was expected to increase from 35% of total building energy use in 2000 to 55% in 2020 (Zhou, 2008).

Within the BEC, space heating belongs to a more general category of heating, ventilation and air conditioning (HVAC), and it very often appears atop of the energy consumption

ranking table. For example, space heating alone accounted for about 50% of total residential energy use in 1998 for the United States (Murtishaw et al., 2001). And in places like China, 65% of BEC was spent on HVAC, while water heating also weighted at 15% (Wu, 2003). The intense energy use from HVAC is probably due to the wider use of air conditioners in China. For example, the percentage of air conditioner (AC) ownership had been more than tripled from 1992 to 2001 in China (Chinese Statistic Yearbook, 2002). In the United States, because of the earlier introduction of air-conditioning, 66.1% of all occupied housing units had AC in 1993, as given by the EIA (1993). Then in 2005, the percentage increased to 84% (EIA, 2005). Due to the increase in air-conditioner ownership, energy consumption by air-conditioning increased from 0.136 to 0.258 trillion kWh from 1993 to 2005 (EIA, 2011). Similar energy use was also observed in Japan. For Japan, spacing heating and cooling was 30% of total energy use in 2007 (Nam, 2010).

1.1.2 Move toward renewable energy

As mentioned above, developing countries like China is experiencing rapid growing energy demand, and with depleting traditional energy sources, they are taking their steps toward renewable energy. Even though the laws promoting renewable and sustainable energy development and consumption came much later than other developed countries, once the laws came into effect, the improvement in renewable energy use was significant (Ma, 2009). For example, in 2005 just before the laws that promoted renewable and sustainable energy development was effective, China's total renewable energy use was only 2.5% of total primary energy consumption (Zhang, 2009). Then in 2006, one year

after the enforcement of the Energy Law, the percentage went up to 7.5% (Chen, 2007). Compared to China, for more developed countries like the United States, renewable energy production was higher at 8.2% of total energy in 2010 (EIA, 2010), but the country was still heavily dependent on fossil fuels (83% of total energy).

1.2 Water source heat pump (WSHP)

1.2.1 Introduction

As mentioned in the previous section, HVAC systems provide food safety and thermal comforts to the users, but at the cost of high energy consumption. In order to lower the total energy use, system efficiency, or coefficient of performance (COP) needs to be improved. Before I discuss details with HVAC efficiency, please review a simplified vapor compression cycle (VCC) schematic, which is mostly used for air conditioning (AC) systems, as shown in Figure 1.

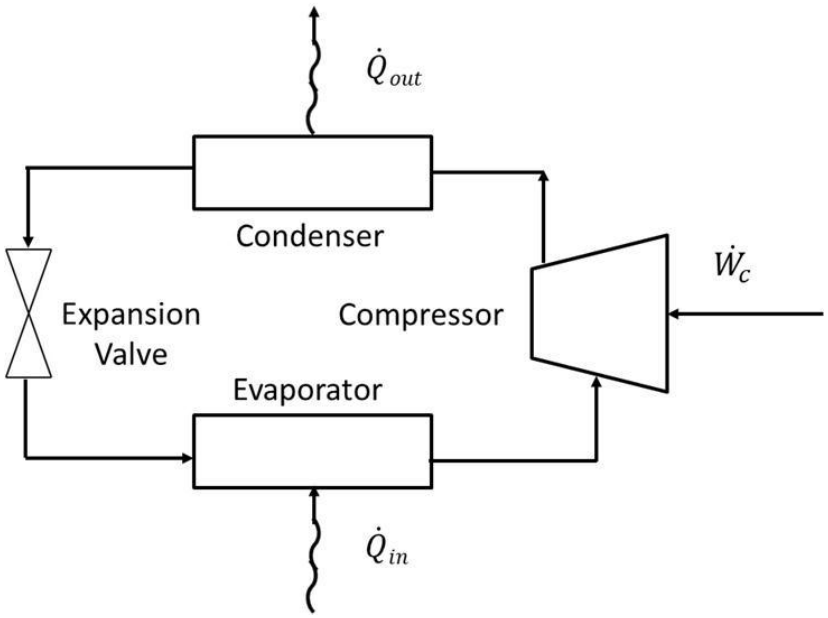

Figure 1: Schematic diagram of VCC

Depending on the application of the VCC system, heat flow direction in the conditioned space changes accordingly. For example, if it is used for cooling, heat is removed from the conditioned space through the evaporator, and then discharged to the ambient through

the condenser. The reverse is true if it is a heat pump. Regardless of the application, in order to raise the overall system coefficient of performance (COP), while providing the same amount of cooling/heating, compressor power needs to be reduced. According to Lee et al. (2012), one way to significantly enhance the system COP is to have a low temperature lift VCC. In general, temperature lift refers to the difference between the evaporation and condensing temperatures of the working fluid, and a smaller temperature lift leads to a smaller pressure ratio (PR) for the compressor, eventually yielding a higher COP. To better demonstrate the benefit of lower temperature lift, heat pump is used as an example.

For the heat pump cycle, condensing temperature/pressure is assumed to be fixed, if evaporation temperature is high, then compressor work can be low and energy consumption is reduced. The concept of low temperature lift heat pump (LTLHP) system using R134a can be seen in Figure 2.

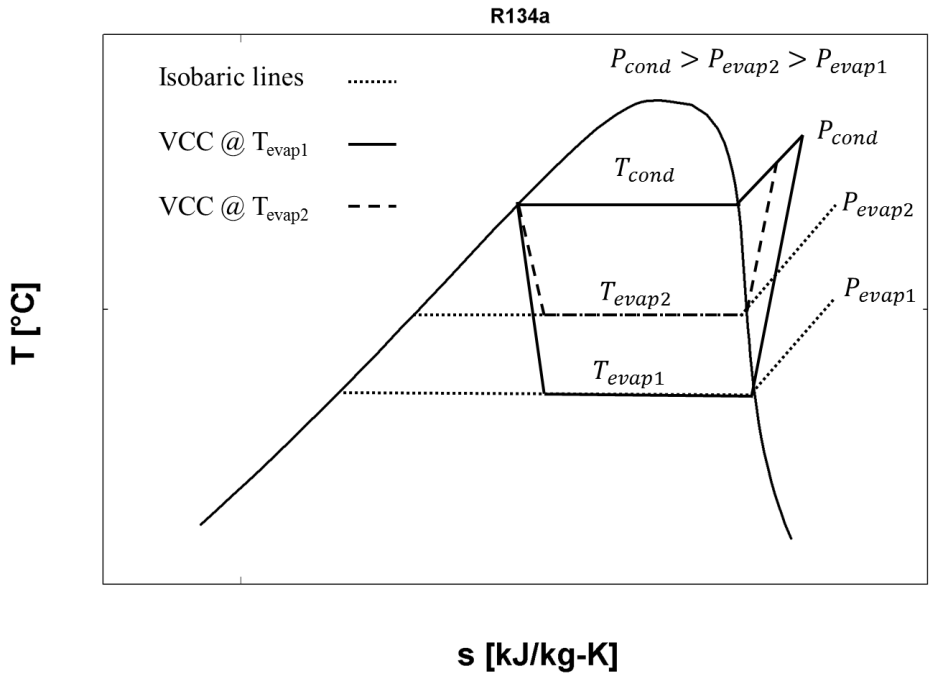

Figure 2: LTLHP with R134a

As shown in Figure 2, a high evaporation temperature (T_{evap2}) leads to a high evaporation pressure, and the pressure difference between compressor inlet and outlet is reduced, which can reduce the compressor work required. Researchers like Wyssen (2011) investigated the effect of a low temperature lift cycle, for the chilled water system he tested COP of 9 was obtained at 20K temperature lift, and then when temperature lift becomes 12.5K, COP improved to 11.5.

For the heat pump system, assuming heat transfer is directly related to difference between evaporation temperature and heat source temperature, if heat source temperature increases, then the required evaporation temperature also increases, which is better depicted in Figure 3.

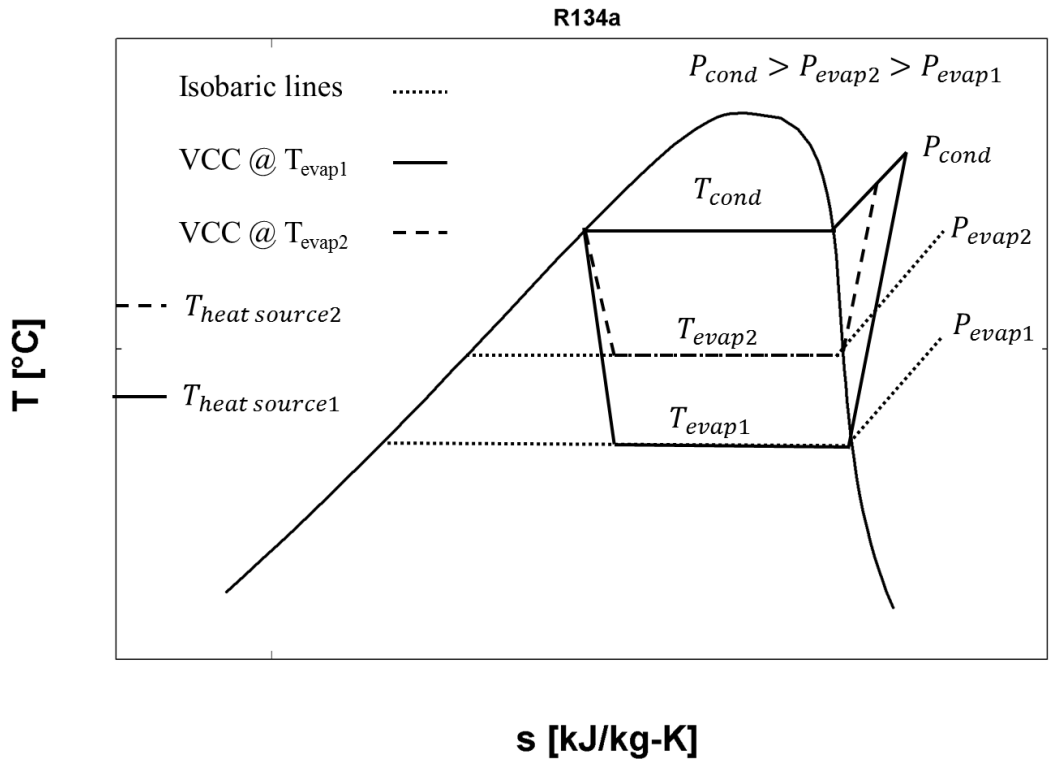

Figure 3: Heat source temperature and evaporation temperature of heat pumps

As shown in Figure 3, a heat source with higher temperature ($T_{heatsource2}$) allows a higher evaporation temperature (T_{evap2}), which in turn increases the evaporation pressure (P_{evap2}) and reduces the pressure ratio. At the end, a LTLHP is realized while the heating capacity remains unchanged. Nevertheless, compared to typical temperature lift heat pumps, LTLHP has smaller temperature difference between heat source and working fluid, and it requires larger flow rate of both heat source and working fluid for the same amount of heat transfer. The increase in flow rate requires a larger capacity pump, and it means higher initial and operation costs to run the system.

1.2.2 Ground source heat pump (GSHP)

As shown in the previous section, for heat pump system, a heat source with high temperature allows a low temperature lift and subsequently reduces the energy consumption. However, most heat pump systems are air source heat pumps (ASHP), and they use ambient air as the heat source. As ambient air temperature follows seasonal changes, it is usually at a very low temperature range in the winter, and therefore, the evaporation temperature cannot increase further for ASHPs. Similar limitation is also true for AC systems in the summer, when ambient air is at a very high temperature range.

In contrast to using ambient air as heat source, ground source heat pump (GSHP) utilizes other forms of heat source, which demonstrates a much more stable thermal level year round. According to ASHRAE (2011), GSHP is a system that uses ground, groundwater or surface water as a heat source/sink. And depending on the type of heat source/sink, GSHP is divided into ground-coupled heat pump (GCHP), ground-water heat pump (GWHP) and surface-water heat pump (SWHP).

Pointed out by Omer (2008), the advantage of using GSHP is based on the fact that, when underground, the Earth is warmer than air in winter and cooler than air in the summer. For example, at depths 1.2m below ground, ground temperature stays between 10 to 13^{o}C all year round. As compared to water, which is the most common heat source/sink for GSHP, air has a much lower thermal mass, making the ASHP system less effective. Also, GSHP is very ideal for floor heating due to its lower temperature than boiler, and floor heating using GSHP can provide better thermal comfort than blasting hot air directly into the conditioned space with conventional heating systems (Omer, 2008).

To better understand the working principles of GSHP, the three different types of GSHP are discussed here. First of all, GCHP forms a closed-loop with a VCC linked to a closed ground heat exchanger buried under the ground. Since it is a close loop system and does not involve water, water quality, quantity and disposal are not a concern (ASHRAE, 1995). Urchueguia et al. (2008) compared a GCHP and an ASHP for both heating and cooling seasons, and the results indicated an energy savings of 43% in heating mode and 37% savings in cooling mode can be achieved with GCHP. Even EPA recognized GCHP among the most efficient and comfortable heating and cooling system available today (EPA).

In contrast to GCHP, GWHP uses inexpensive wells as the heat source/sink, and it extracts large quantity of water out of the extraction well and then discharges water back to the re-injection well, making it an open-loop system (ASHRAE, 1995). In places like China, GWHP is widely used in cold climate zone, according to Yang et al. (2010), and it is currently the most widely used GSHP in China. Compared to ambient air, well water demonstrates a more preferred temperature profile. For example, Paksoy et al. (2004) utilized groundwater in a cold well at 18^{o}C for air conditioning of a supermarket in Turkey, compared to the ambient air at 30 – 35^{o}C in the summer. Then the waste heat was stored through the warm well, which was recovered in the winter. The integration of cold and warm wells made the system 60% more efficient than conventional systems.

Compared to GCHP and GWHP, SWHP is more versatile and it can be either closed-loop or open-loop system. A closed-loop SWHP consists of water-to-air or water-to-water heat pumps connected to piping network submerged in a water body such as river or lake, and

either water or water-antifreeze solution flows through the piping loop under the water. Heat is transferred from the water body to the heat pump as a result. Open-loop SWHP is more constrained to water temperature, and its application is preferred in warm climate. In that case, water can be pumped either directly to the heat pump or through an intermediate heat exchanger that is connected to the heat pump (ASHRAE, 2011). In general, temperature of surface water is also more stable than ambient air. For example, Chen et al. (2006) studied an open-loop heat pump system using the water from Mengze Lake in Hunan, China. They found the water temperature to be 2 – 5K lower/higher than air temperature during most time in cooling/heating season, and sometimes the difference can be as high as 8K. Such significant temperature difference indicates surface water's potential to achieve LTLHP and energy saving.

Regarding the benefit of using surface water as a heat pump's heat source/sink, Buyukalaca et al. (2003) conducted a study to compare the SWHP to ASHP for both heating and cooling seasons in Turkey, where ASHP was the most widely used. One common problem with ASHPs, as they pointed out is that, in the winter when outside temperature drops below critical temperature frosting on the evaporator is possible. When that occurs, the heating capacity and performance could drop significantly and thermal discomfort is the direct result. In order to investigate potential use of the rich water resources in Turkey, they first monitored annual thermal profile of the Seyhan River in Turkey. And then they ran an experiment to test the heat pump performance using both water and air, and attained 15-40% higher COP with water-source than air-source for heating, and 35-40% higher for cooling. Improvement in COP was also found by Chen et al. (2006), where they used lake water as a heat source/sink. Even under the same heat

source/sink temperatures, WSHP has COP 0.7 - 0.85 higher than ASHP in cooling season and 0.46 higher for heating season.

1.2.3 Seawater heat pump

Apart from GSHP, seawater is another heat source/sink that has been widely investigated. Pointed out by Zhen et al. (2007), seawater heat pump is particularly suitable for coastal areas like Dalian, China, to provide district cooling and heating (Zhen, 2007). In the winter, water temperature is high enough to be used for seawater source heat pump, and in the summer, seawater temperature is low enough to be used for cooling. The advantage of seawater over ambient air is quantified by Song et al. (2007), where they measured the seawater and ambient air temperature in Nagasaki, Japan from April, 2000 to December 2001, and the temperature profile can be seen in Figure 4.

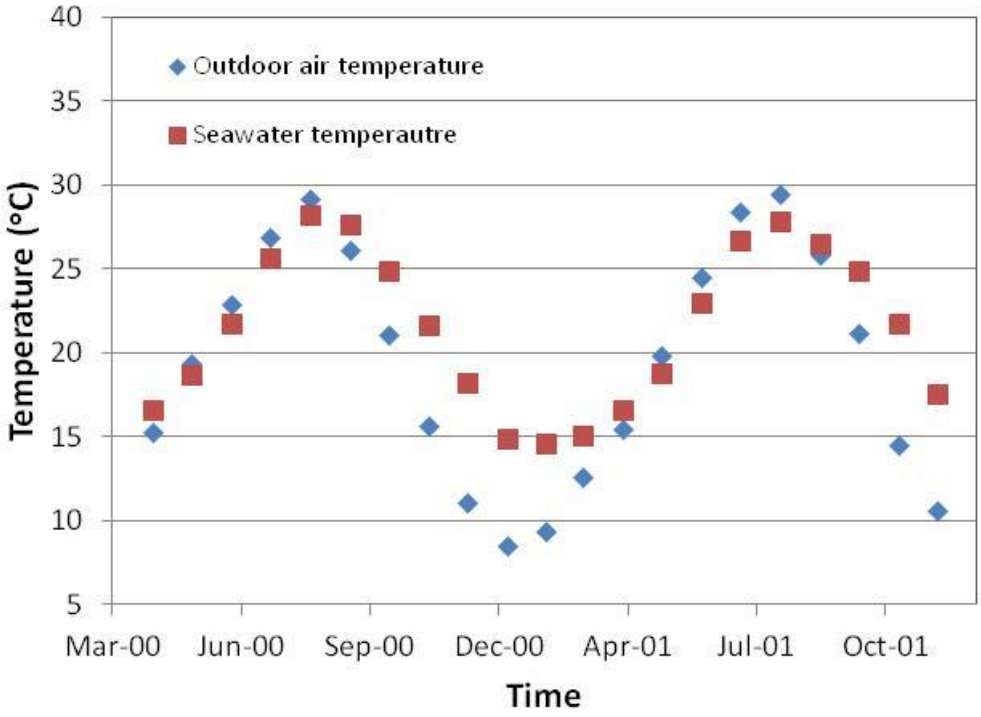

Figure 4: Outdoor air and seawater temperatures in Nagasaki, Japan (Song et al., 2007)

As shown in Figure 4, in the summer months, seawater was colder than ambient air, and in the winter, seawater had higher temperatures, making it a better heat source/sink than ambient air.

Other places like Hong Kong, where it is surrounded by seawater is also ideal for seawater heat pump application. As suggested by Yik et al. (2001), in the summer, buildings near the Victoria Harbor in Hong Kong can take advantage of the cooler seawater (27^{o}C) and convert from air-cooled (35^{o}C) air-conditioning system (AACS) to water-cooled air-conditioning system (WACS), resulting in a significant energy reduction. Moreover, for buildings further away from the harbor, seawater supply system is needed as a trade-off. The conversion from AACS to WACS was also discussed by Al-Marafie et

al. (1986), where they found WACS achieved energy savings of 24% over AACS for residential buildings, and 25% for non-residential buildings.

On the other hand, Song et al. (2007) carried out a comparison study on the performance of indirect seawater heat pump cooling, cooling tower system, air cooling chiller system and direct seawater heat pump cooling in a commercial complex where only cooling is needed. At the end, they concluded indirect seawater heat pump has the highest COP, due to a lower condensing temperature. Instead of utilizing seawater for cooling, Okamoto (2006) collected the heat from seawater and used it as a heat source for the heat pump, and energy saving was achieved over ASHP or oil fired system.

Despite the promising energy saving from seawater source heat pump, there are certain limitations imposed on its application. For instance, in cooling applications there is regulation on how much the discharge seawater temperature from open-loop system can be warmer than ambient water (Zhen, 2007); if the discharge water temperature is too warm, there could be severe impact on the surrounding marine system. Additional concern rises from seawater quality, and the heat exchanger in direct contact with the supply seawater is subject to water fouling, corrosion and blockage (Omer, 2008). So if possible, fresh water is always preferred whenever it is available (Yik, 2001). However, for places like Hong Kong where fresh water is very scarce and prohibited for cooling use, corrosion from seawater can be minimized by using indirect seawater system. In this case, stainless steel or titanium PHE are often used and fresh water is the intermediate medium to transport heat from condenser to seawater for the case of cooling.

1.2.4 Waste water source heat pump

Besides using energy stored in the natural environment, like those discussed in the above sections, daily waste water also contains vast amount of thermal energy that can be extracted. In the past, waste water reuse was mainly found in agriculture (Urkiaga, 2006), but nowadays the possibility of energy recovery from waste water is gaining more attention.

For example, for the sewage alone, thermal energy lost can be up to 15% of total energy provided in a conventional new building (Schmid, 2008), and it presents great potential for energy recovery. Compared with heat sources like ground water or ambient air, waste water from local residential drainage systems stays at a relatively high temperature in the winter, making it very suitable as the heat source for heat pumps. This is better demonstrated from the work done by Funamizu et al. (2001). In their study, they measured the tap water from Sapporo, Japan to be 3.8^{o}C in February 1998, then after water usage, the waste water temperature increased to 13.1^{o}C, and it was even heated up to 13.8^{o}C coming out of the waste water treatment plant (WWTP).

In terms of a country, in Switzerland about 6,000 GWh of thermal energy is lost via sewage, and this corresponds to around 7% of thermal energy demand for space heating and hot water generation (SwissEnergy, 2005). In other places like Japan, Funamizu et al. (2001) estimated heat energy in waste water or treated water is about half of total energy wasted in Sapporo, Japan. And in Tokyo overall, about 38,000 TJ of heat energy is wasted in the sewage system annually, which is equivalent to 0.4 million households' heating and cooling loads.

Waste water is generated through many different ways, and generally speaking, waste water usage is divided into three sectors: household/municipal, industry and agriculture (Yang, 2007). Based on predictions, in the future, household/municipal sector will make the largest contribution to the increase of waste water discharge. Depending on the waste water quality, Chu et al. (2004) suggested waste water reuse from three major sources: released treated waste water within factories after meeting quality standard requirement, through waste water treatment plants (WWTPs), and decentralized on-site waste water treatment facilities. Examples of decentralized on-site waste water treatment facility can be found in cities like Beijing, China, where it is required for certain residential communities to have their own on-site waste water treatment facilities.

Slightly different from the proposal by Chu (2004), Schmid (2008) also proposed three ways to extract thermal energy from sewage water: in-house energy recuperation, recovery in sewer or from cleansed waste water coming out of WWTP. The three schemes are better depicted in Figure 5.

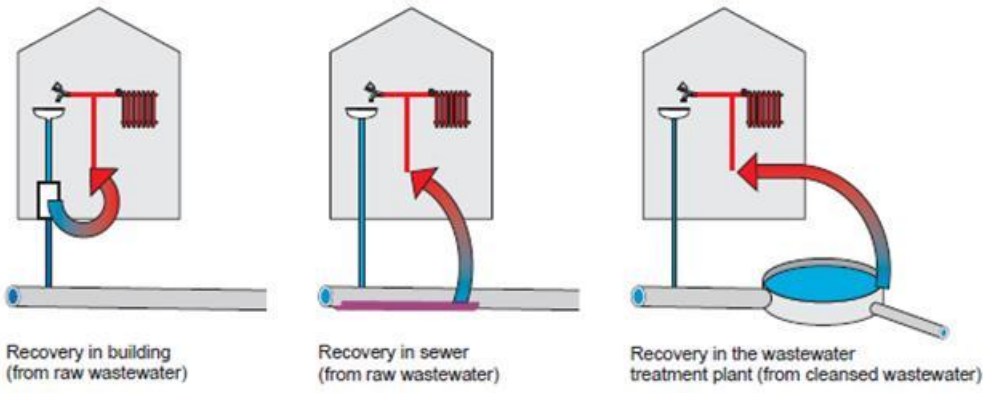

Figure 5: Waste water recovery schemes (Schmid, 2008)

Analyzed by Schmid, among the three options energy potential from the cleansed waste water is the highest, since it has the highest temperature. Also, effluent from WWTP usually presents a lower potential of clogging, than untreated waste water, and reducing the cost of maintenance (Tassou, 1988). However, most WWTPs are located predominantly in remote areas, which are very far away from available customers, and the best use of the cleansed water is for the plant itself.

Use of WWTP waste water was further discussed by Funamizu et al. (2001), in which they listed in details the projects in Japan started in 1987, which had been using effluent from WWTP to provide heating and cooling. For example, Ochiai WWTP used its own secondary effluent to provide heating of the administration buildings, yielding 25% energy savings compared to conventional boiler system for heating in March 1987. For very remote WWTP, Tassou (1988) suggested that the heat recovery from effluent can be coupled with surrounding developing industry, which can make good use of this cheap source of heat.

Depending on its configuration, waste water source heat pump (WWSHP) can be identified as either direct or indirect type, as stated by Shen et al. (2012). For direct type, heat transfer takes place between waste water and refrigerant directly inside the evaporator, and the evaporator is greatly affected by the waste water quality. In indirect type, waste water and refrigerant are separated by an intermediate medium like fresh water, and heat transfer between waste water and refrigerant is conducted by that medium. One of the common used WWSHPs is the urban sewage source heat pump (USSHP), which can be used for both heating and cooling. When used for heating, as summarized

by Zhao et al. (2010), sewage water is first sent to the waste water heat exchanger, and heat is taken from the sewage and sent to the evaporator as low grade heat source, then heat is released through the heat pump's condenser as high-grade heat. In Zhao's study (2010), energy savings of 42% was obtained in the heating season, compared to a conventional boiler.

USSHP may be particularly applicable for large scale public showers, whose waste water has higher temperature than normal urban waste water, as suggested by Liu et al. (2010). In addition, public bath facilities have very concentrated heat use and heat elimination, and the demand is stable throughout the year. To further investigate the possibility of reusing the public shower waste water, a system was built to harvest heat from waste water and used it for domestic hot water (DHW) application; in this case it served to provide hot water for the public bath facilities. Because of the low contamination level of public bath facility's waste water, this waste water also belongs to a category of water called grey water. Defined by Al-Jayyousi (2003), grey water is water collected separately from sewage flow that originates from laundry and showers. Since it is only slightly contaminated by human activities, and it can be reused after certain treatment. Similar work was done by Baek et al. (2005), who designed a compression heat pump system operated with waste water from sauna and public baths in Yoseong area in South Korea. Ran by the off-peak electricity, heat was charged into hot storage tank at night. Then hot water storage tank provided hot water for the shower. The designed system had a mean operating COP of 4.5 to 5.0, which was higher than ASHP.

The use of heat recovery for hot water generation was appraised by Meggers et al. (2011). As they pointed out, very often hot water demand is not affected by thermal improvement in buildings, and the most efficient way to reduce energy spent for DHW is to recover heat loss from waste water, such as recovery of waste water discharged directly out of the building.

Nevertheless, similar to seawater heat pumps, water fouling inside the heat exchanger for waste water heat recovery is the main obstacle to be solved (Schmid, 2008), as well as the many kinds of contaminant waste water contains. Moreover, unlike seawater, waste water is a finite source of energy, and it heavily depends on the water usage in buildings. In order to make the waste water energy harvesting economically feasible, there needs to be a continuous supply of waste water at large quantity. Even for heavily used buildings which can provide large quantity of waste water when in use, there will be a significant drop in availability of waste water during weekends or holiday seasons, and building occupancy is another factor that can affect waste water supply.

1.3 Plate heat exchanger (PHE)

For all the WSHP works discussed in the previous section, it was confirmed by many researchers that they show better performance than ASHP, and energy saving can be achieved. As the heat source is changed from air to water, the evaporator also has to be changed. One very suitable candidate for such water-to-refrigerant application is PHE.

1.3.1 PHE overview

Compared to other heat exchangers such as shell-and-tube heat exchanger, which is also applicable for liquid-to-liquid heat transfer, PHE are usually more compact, flexible and effective. Due to their complex geometry, it is easier for turbulence to occur (Huang, 2012). Also pointed out by Faizel et al. (2012), PHE has the advantage of high thermal effectiveness, large heat transfer area per volume, low weight and possibility of heat transfer between many streams. In addition, corrugation on the plate surface can induce secondary flow and causes turbulent mixing, which allows fluid elements to have effective heat transfer with adjacent channels.

As summarized by Ayub (2003), there are several types of PHEs available, including conventional gasketed plate-and-frame, brazed plate heat exchanger (BPHE), shell-and-plate and semi-welded PHE. Inside a gasketed plate-and-frame type, all the plates are sealed by elastomer gasket, as shown in Figure 6. Even though gasketed plate-and-frame type is very easy to assemble and disassemble, gasket material is subject to the corrosive refrigerant and leakage is possible. In contrast, BPHE has all its plates brazed together (Figure 7), giving it the strength to resist much higher pressure and corrosion. Shell-and-plate type is the newest design, and it contains a plate pack that is welded together and inserted inside the shell. The plate pack can be seen in Figure 8.

Figure 6: Gasketed plate-and-frame PHE (Alfa Laval, 2012)

Figure 7: BPHE (FlatPlate, 2012)

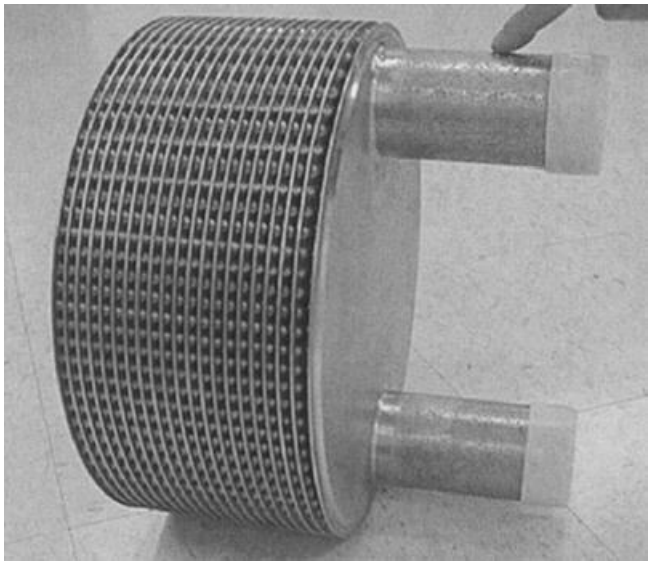

Figure 8: Shell-and-plate (Ayub, 2003)

As pointed out by Ayub (2003), initially, gasketed plate-and-frame type was very ideal for single phase liquid-to-liquid application, in which pressure range was relatively low. When operating pressure becomes very high, such as for HVAC application, gasket itself presents as a potential site for leaking, due to its mechanical weakness. This raised serious concern, especially when it comes to refrigerant leakage for HVAC industries, making the application in two-phase heat transfer very uncommon (Huang, 2012). The problem remained until the invention of BPHE and semi-welded PHE. In a BPHE, multiple plates are brazed together and the possibility of any leakage is eliminated. However, once the plates are welded together, it is almost impossible to make changes such as adding more plates, without causing any damage to the assembly, as depicted in Figure 7. In order to cope with both leakage and flexibility, I selected the semi-welded plate design, which can sustain higher pressure than gasketed plate-and-frame, and is easier to modify than BPHE.

1.3.2 Semi-welded PHE

Different from the regular gasketed plate, in semi-welded PHE design, two identical plates are first laser welded together (Figure 9) to form an interior flow channel for the refrigerant side, as shown in Figure 10. The two plates welded together are now called a single cassette (Ayub, 2003). Refrigerant flow through every cassette is still connected by the refrigerant-side gaskets, and these gaskets separate the refrigerant side from the water side. The refrigerant-and water-side gaskets can be better seen in Figure 9.

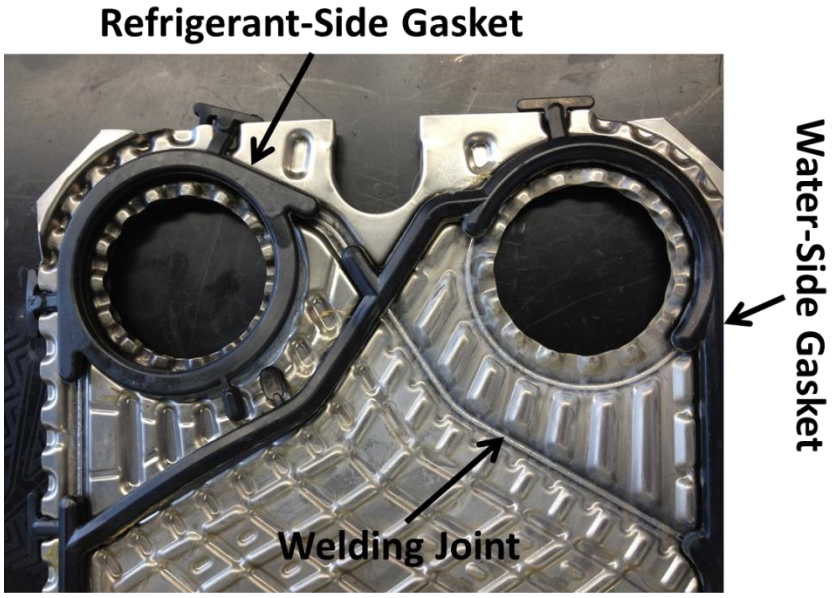

Figure 9: Gasket and welding

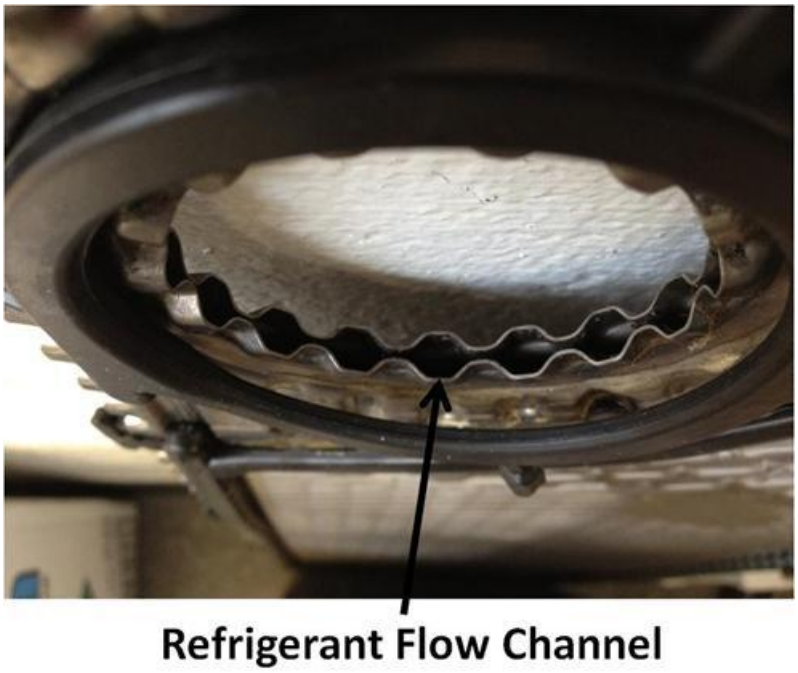

Figure 10: Refrigerant flow channel

1.3.3 PHE geometrical parameters

As mentioned before, PHE generally has better heat transfer than other types of heat exchangers, and this is mainly due to its complex geometry on the plate surface. One type of geometry found regularly is the chevron type, and it is denoted by its sinusoidal shape corrugations, as shown in Figure 11.

Figure 11: Sinusoidal shape corrugation

Indicated by Yan et al. (1999), the corrugation helps to induce turbulent flow even at low Reynolds number (Re), as well as to increase heat transfer area and to distribute fluid flow evenly. Another explanation was given by Han et al. (2010), where they pointed out corrugated plates are very irregular and the flow region is continuously contracting and expanding, forcing the flow to change direction all the time, and allowing turbulent flow to occur more easily. This is further elaborated by Faizal (2012), where he pointed out for smooth surface, once hydraulic layer is fully developed, central region of the flow does not receive heat from the wall, whereas corrugation can induce secondary flow to enhance heat transfer.

Regarding the chevron corrugation for PHE, Ayub (2003) described several geometry parameters of particular interest, and they all affect the overall heat transfer

characteristics. First of all, plate length (L_p) and width (w) of a typical PHE with chevron corrugation are denoted in Figure 12, as well as the chevron angle (β).

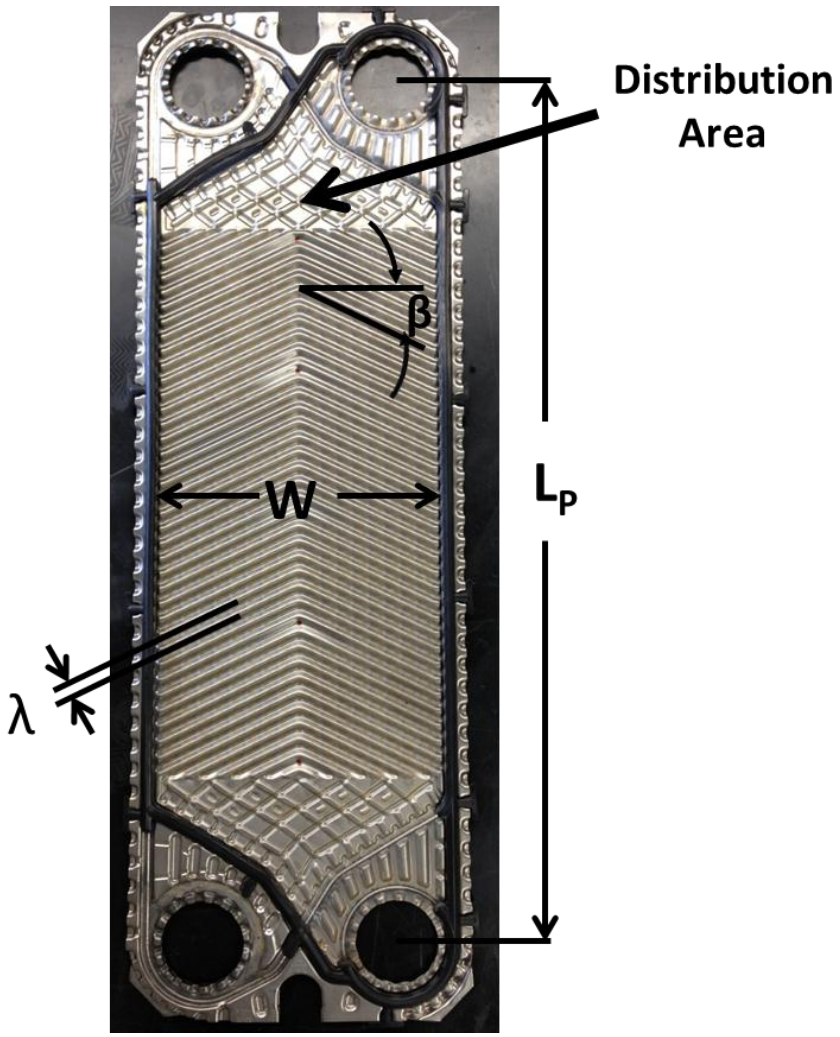

Figure 12: Dimension/Parameters of chevron type PHE

As drawn in Figure 12, chevron angle (β) is defined as the angle between the corrugation and the direction perpendicular to the flow. According to Martin (1996) and Khan et al. (2012), depending on how the chevron angle affects heat transfer performance and pressure drop, different chevron angles can be called soft or hard chevron angles. Different from the configuration used here, in both studies the chevron angle was defined

as the angle of corrugation relative to direction of flow. In their studies, they indicated a high (60^o) chevron angle in their definition has better thermal performance and higher pressure drop, and it is said to be a hard chevron type. Due to the different definition, in this study, a low chevron angle (30^o) is actually equivalent to the hard (60^o) chevron angle in the previous two studies, and it provides high thermal efficiency, at the cost of high pressure drop. In addition, corrugation pitch (γ) is defined as the distance between adjacent corrugations.

Then corrugation depth (b) is defined. As shown in Figure 13, corrugation depth (b) is the actual space available for flow, taking into account the finite plate thickness (Eq. 1.1).

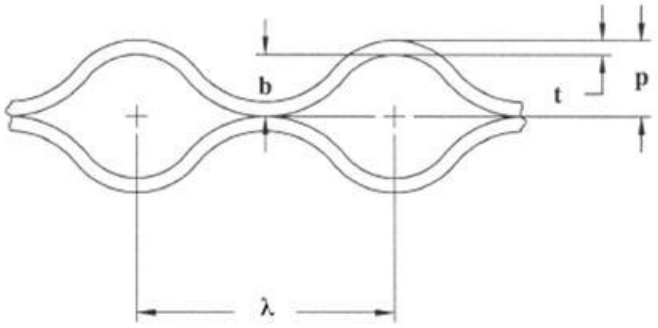

Figure 13: Corrugation depth (Ayub, 2003)

$$\mathbf{b = p - t} \qquad \text{Eq. 1.1}$$

Once corrugation depth (b) and plate width (w) are known, actual cross sectional area (A_x) is defined as:

$$A_x = wb \qquad \text{Eq. 1.2}$$

Another parameter of importance is the enlargement factor (ϕ). As explained by Ayub (2003), enlargement factor is the ratio of the developed length to the protracted length (Figure 14). However, if the developed length is not known, Fernandes et al. (2007) provided an estimation formula of enlargement factor based on channel aspect ratio (γ) (Eq. 1.3) and chevron angle (β), as calculated in Eq. 1.4.

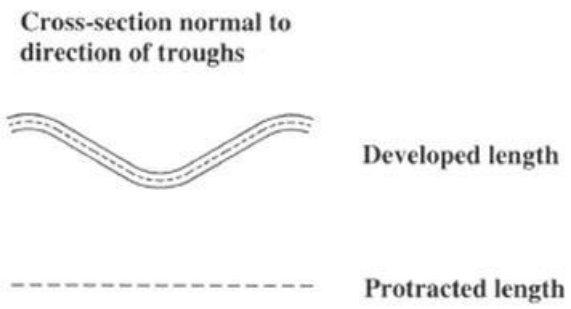

Figure 14 Developed and protracted length (Ayub, 2003)

$$\gamma = \frac{2b}{\lambda} \qquad \text{Eq. 1.3}$$

$$\phi = \frac{1}{6}\left[1 + \left\{1 + \left(\frac{\pi}{2\cos(\beta)}\right)^2 \gamma^2\right\}^{0.5} + 4\left\{1 + \left(\frac{\pi}{2\sqrt{2}\cos(\beta)}\right)^2 \gamma^2\right\}^{0.5}\right] \qquad \text{Eq. 1.4}$$

At the end, hydraulic diameter (d_e) is simply based on cross sectional area (A_x) and perimeter (P):

$$d_e = 4A_x/P \qquad \text{Eq. 1.5}$$

When corrugation depth is much smaller than plate width, perimeter is estimated as (Ayub, 2003):

$$P = 2(b + \phi w) \approx 2\phi w \qquad \text{Eq. 1.6}$$

So hydraulic diameter is given as:

$$d_e = \frac{2b}{\phi} \qquad \text{Eq. 1.7}$$

1.3.4 PHE heat transfer performance

The evaporative heat transfer inside a PHE has been investigated by many researchers, and there has been a lot work done to understand its mechanism. For example, Huang (2012) conducted tests on evaporative heat transfer of R134a inside a chevron type BPHE. And the effect of heat flux, mass flux, outlet vapor quality, and chevron angle on evaporation heat transfer coefficient (HTC) were tested. As a result, he found that the HTC had a strong dependence on heat flux, but a weak dependence on refrigerant mass flux, vapor quality, and the chevron angle. Based on the results, he suggested that nucleate boiling is the dominant mode, which is controlled by heat flux. Djordjevic et al. (2008) also conducted a study on the evaporation heat transfer for flow boiling of R134a in a chevron-pattern corrugated frame and plate PHE. Different from Huang, thermocouples (TCs) were inserted into the water-side plate to measure the local temperature of the wall and the water, hence local heat transfer and vapor quality on the refrigerant-side can be both calculated. At the end, they observed a strong increase in

HTC when vapor quality increases to about 0.2. And when vapor quality becomes higher than 0.4, further rise in heat flux only yield to small increase in heat transfer; showing nucleate boiling was not dominant.

Similar to Djordjevic et al. (2008), Yan et al. (1999) tested the effect of vapor quality on evaporation heat transfer inside a PHE. However, in their study, they utilized a pre-heater to control the inlet vapor quality into the evaporator, and with a fixed amount of heat added to the evaporator, the mean vapor quality within the PHE evaporator can be well controlled. As it turned out, HTC increased with vapor quality for all tests. At low quality regime, effect of mass flux on heat transfer was insignificant, and then became more significant for higher vapor quality.

Instead of R134a, Han et al. (2003) tested evaporative heat transfer of R410A and R22 inside a BPHE, and mass flux, evaporating temperature, vapor quality, heat flux, and chevron angle were varied to determine their effects. At a given mass flux, they found HTC increased with vapor quality and decreased with evaporating temperature. For low vapor quality region, they found heat transfer more sensitive to heat flux, and this was because nucleate boiling was more dominant than convective boiling. Hsieh et al. (2003) also studied evaporation heat transfer of R410A inside a PHE, and they found the heat transfer was insensitive to mass flux at low vapor quality. Then when the mass flux was high, there was a larger increase in heat transfer with quality.

Even though the exiting research conducted on PHE evaporation heat transfer is very extensive, there is limited work done for low refrigerant mass flux conditions specifically.

Moreover, the application of PHE toward LTLHP is very rare, as well as using PHE for heat recovery from heat sources like waste water or seawater.

1.4 Refrigerant selection

When refrigerant was first used for refrigeration and air conditioner systems, its damage to the ozone layer and contribution to global warming were not realized. To better quantify those two measures, researchers defined ozone depletion potential (ODP) and global warming potential (GWP). According to Calm et al. (2001), ODP is a normalized based on a value of 1.000 for R-11, and it indicates the refrigerant's ability to destroy the ozone layer. On the other hand, GWP is relative to carbon dioxide, and it measures the ability to warm the planet by acting as greenhouse gas.

Among the many types of refrigerants available in the market, refrigerant R22 has been used for residential heat pumps and air conditioning systems for more than four decades, because of its high energy efficiency (Karagoz, 2004). However, R22 is a hydrochlorofluorocarbon (HCFC) refrigerant, with ODP of 0.034, GWP of 1,780 and life span of 12.0 years (Calm et al., 2004), and it is scheduled to phase out completely by 2030. So far, R134a, a type of hydrofluorocarbon (HFC) refrigerant, is one of the candidate replacements for R22. Compared with R22, R134a has zero ODP and GWP is 1,320, and its life span (14 years) is almost the same as R22 (Calm, 2004). In terms of performance, Karagoz (2004) conducted a comparison study between R22 and R134a for an air-to-water vapor compression heat pump. For the range of conditions he tested, COP of pure R22 was in the range of 1.1 to 3.1, while that of R134a was higher, and it was from 2.2 to 3.7.

Other than R22, R134a was also considered by researchers like Carpenter (1992) and Preisegger (1992) as a replacement for R12 for a wide range of refrigeration and air-conditioning applications. R12 a chlorofluorocarbon (CFC) refrigerant, and it had been used in most domestic and commercial refrigeration units since 1930s (Carpenter, 1992). But in terms of damage to the environment, R12 has ODP of 1 and GWP of 2,400, and a very long life of 100 years, which makes it more harmful than R134a (Halimic, 2003). Regarding operation pressure, R134a is a medium pressure refrigerant, making it very suitable for semi-welded PHE, and it can also replace R12 in domestic refrigeration and automobile air conditioning (Longo, 2010).

1.5 Objectives of study

Based on the literature review, I believed that energy consumption toward HVAC application is increasing year by year, and it is very difficult to lower heating or cooling demand without affecting the indoor thermal comfort. On the other hand, if the system efficiency can be further improved, then total energy use can be reduced, and this is possible through a low temperature lift HVAC system. For the case of heating, in order to reduce the temperature lift, instead of ambient air, a different heat source is required - one that, has higher temperature level than air. Some of the possible alternates discussed in the literature are ground water, seawater and waste water. WSHPs utilizing those heat sources all demonstrate better performance than ASHP. Since the heat source is changed from ambient air to water, I recommend the use of a semi-welded PHE to be used as the evaporator. Many researchers have discussed evaporation mechanism inside a PHE, and there was limited study done on the application of PHE on LTLHP systems. Since the

LTLHP requires a large water flow rate, the water-to refrigerant PHE is operated at lower refrigerant mass flux than typical operating conditions investigated by other researchers. Also, due to its low ODP and GWP, I selected R134a as the working fluid in this study. Throughout this study, I investigate evaporation heat transfer characteristics of R134a inside a semi-welded PHE, and discuss the effects of different refrigerant mass fluxes (1.28 and 1.70 kg/(m^2s)), evaporation pressures (683 and 533 kPa), heat fluxes (110 and 190 W/m^2), and vapor qualities (0.15 to 0.95) on the evaporation HTC.

Chapter 2. Experimental Apparatus and Procedure

2.1 Test heat exchanger

The semi-welded PHE used in this study composed of a total of 8 cassettes, which is better shown in Figure 15.

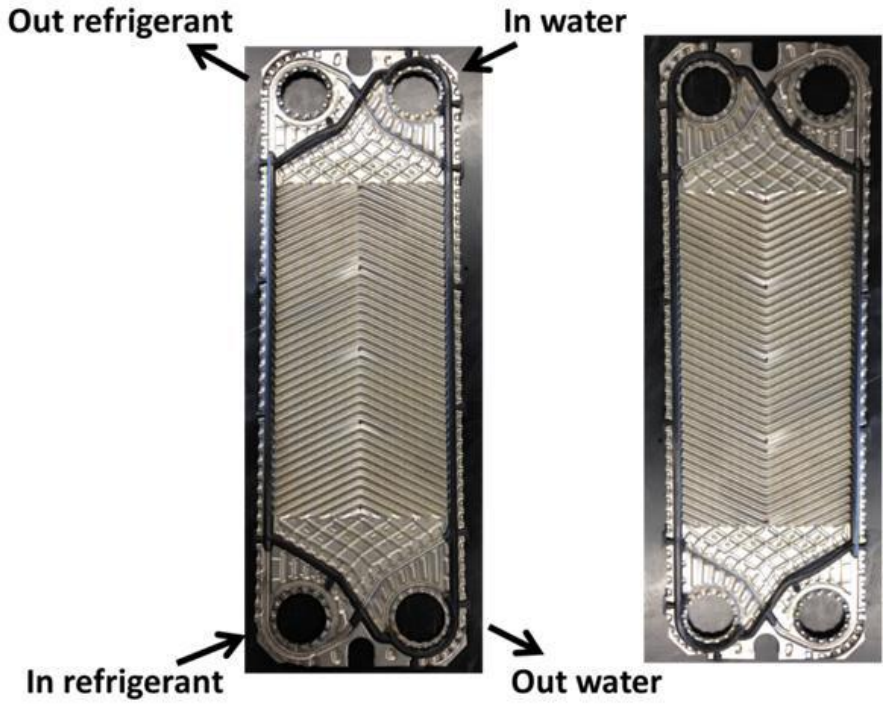

Figure 15: Tested PHE cassette (left: cassette front, right: cassette back)

As shown in Figure 15, both water and refrigerant have their inlets and outlets on the same side and such configuration is called a parallel flow (Alfa Laval, 2012). As mentioned in the previous section, since the two plates making up the cassette are identical, the front and back plates have the chevron angle pointing in the opposite directions. Detailed description and geometrical parameters of the chevron-type plate are summarized in Table 1.

Table 1: PHE details

Manufacturer	Alfa Laval
Model	M6-MWFD
Maximum Allowable Working Pressure (kPa)	1,724
Plate Length Lp (m)	0.648
Plate Width w (m)	0.210
Corrugation Pitch λ (mm)	9.5
Chevron Angle β (^{o})	30
Enlargement factor φ	1.346
Corrugation depth b (m)	0.0028
Hydraulic Diameter d_e (m)	0.00416
No. Cassette	8
Plate Material	Titanium
Plate Thermal Conductivity k (W/m·K)	21.9
Weight of Plate (kg)	1.1
Plate Thickness t (m)	0.0006
No. of Heat Transfer Surfaces	14
No. of Refrigerant Channels	8
No. of Water Channels	7
Heat Transfer Area per plate (m^2)	0.124
Total Heat Transfer Area (m^2)	1.736
Refrigerant Flow Area (m^2)	4.69E-3
Water Flow Area (m^2)	4.11E-3

As shown in Table 1, there are eight cassettes and hence eight refrigerant channels, but only seven water channels; this is due to the absence of water flow between the two end plates and the frame holding the plates together.

2.2 Test facility

2.2.1 Refrigerant loop

An existing facility was modified to evaluate the evaporation performance of PHE, under the specified operating conditions. Schematic of the facility can be seen in Figure 16.

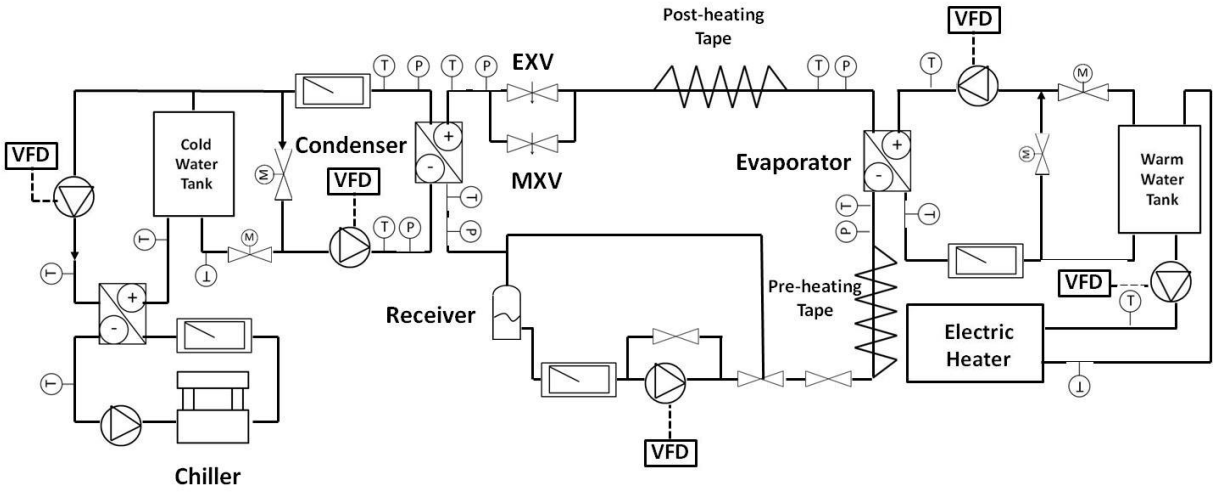

Figure 16: Test facility

Different from a conventional VCC, the facility was originally built for a power cycle, in which the evaporators were on the higher pressure side, wherein a VCC has the condenser on the high pressure side. For the purpose of this study, the evaporators were tested as if it was in a normal VCC, except having the condenser on the lower pressure side. Furthermore, instead of having a compressor, sub-cooled refrigerant was pushed by a diaphragm pump, whose maximum flow is 127 cm^3/s at a pressure of 689 kPa, as

shown in Figure 17. And it is controlled by a variable frequency drive (VFD) controlled motor, with maximum output power of 0.75 kW.

Figure 17: Refrigerant pump

After exiting the pump, refrigerant went through a section of stainless steel piping, which was wrapped around by a section of heating tape (Figure 18) for pre-heating purpose, before entering the evaporator. Both heating tape and stainless steel pipe were insulated by glass fiber to minimize heat loss to the ambient, as shown in Figure 19.

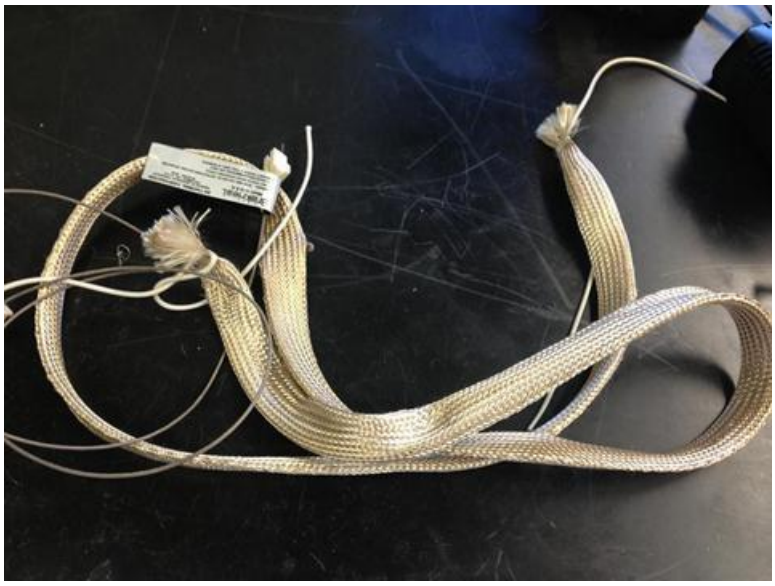

Figure 18: Heating tape

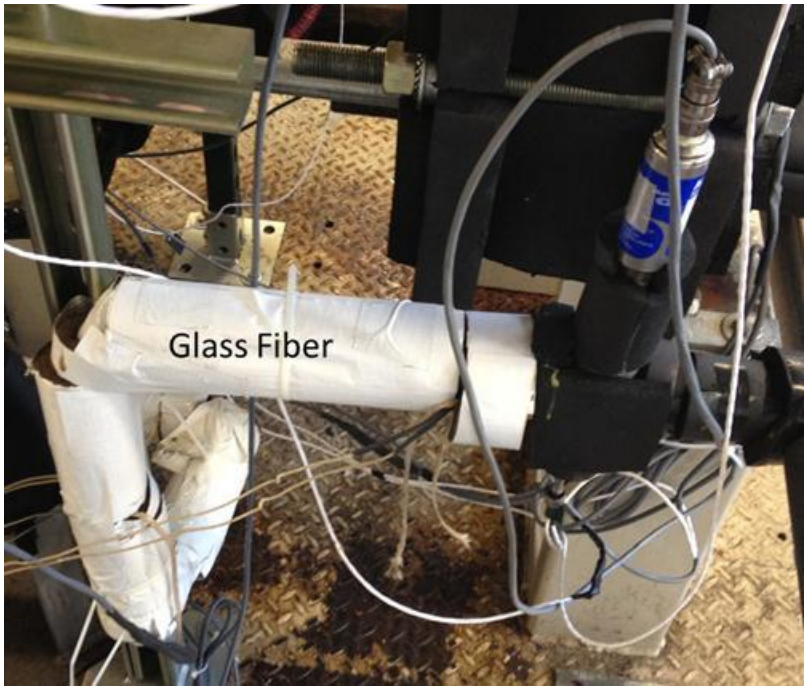

Figure 19: Insulation for heating tape

Counter flow heat transfer is selected to be the flow pattern of the evaporator, and piping configuration was made to accommodate such flow. And similar to the pre-heating tape,

the entire refrigerant loop was heavily covered by Armacell insulation, including the PHE, as shown in Figure 20.

Figure 20: Insulation installed

After going through the evaporator, another heating tape was attached after the outlet for post-heating purpose. Sufficient heat was added to make sure the refrigerant was fully evaporated and reached superheated state, before making its way to an electric valve actuator (Figure 21), which controlled opening of a valve, and the pair acted as an electric expansion valve (EXV). With the use of an EXV, evaporation pressure can be well controlled.

Figure 21: EXV and its actuator

After the refrigerant expanded through the EXV, it entered the condenser, which was also a PHE, but a semi-welded PHE of different plate pattern from the evaporator used. The sole purpose of the condenser was to complete the cycle, and provide sufficient cooling to fully condensate the refrigerant, making it a sub-cooled liquid.

Then sub-cooled refrigerant went into a receiver tank, and the tank fed liquid refrigerant to the pump. Because of the high and stable density of liquid refrigerant, the mass flow rate of the cycle was measured very accurately by a Coriolis mass flow meter installed at the inlet of the pump, as shown in Figure 22. The whole cycle completed when the subcooled refrigerant reentered the pump.

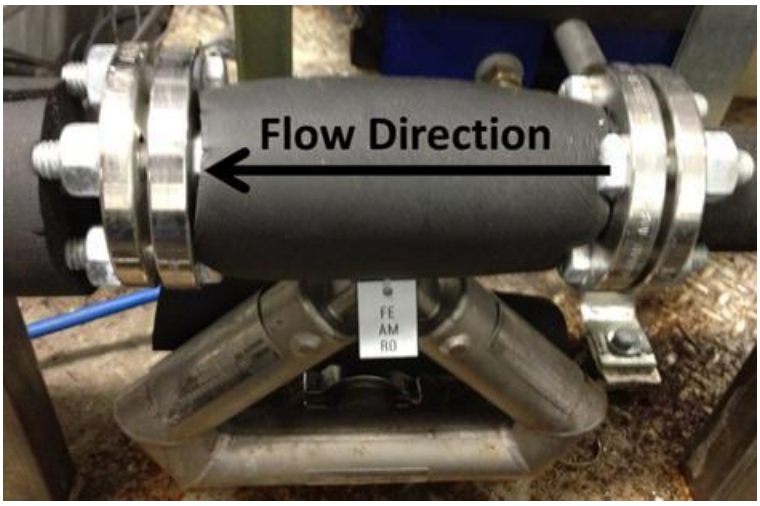

Figure 22: Coriolis mass flow meter for refrigerant

2.2.2 Water loop

As mentioned above, there were two PHEs in the system, one for condenser and one for evaporators, and both of them were used for refrigerant-to-water heat transfer. For the condenser, chilled water was taken from a cold water storage tank (Figure 23), and the cold water was generated using a separate water to water/glycol PHE, as shown in Figure 24. On the other end, water/glycol was fed to an outdoor chiller (Figure 25), which provided maximum cooling capacity of 105.3 kW for the entire system.

Figure 23: Cold water storage tank

Figure 24: Water-to-water/glycol PHE

Figure 25: Outdoor chiller

With regards to the warm water-side, there was a separate warm water loop. Similar to the condenser, warm water going into the evaporator was taken from a warm water storage tank, and the heat is added by an electric heater with maximum heating capacity of 54 kW, as seen in Figure 26.

Figure 26: Warm water loop

In order to better control the evaporation process, inlet water temperature was very critical and needed to be controlled, and I did this by using a pair of electric actuator, as shown in Figure 27.

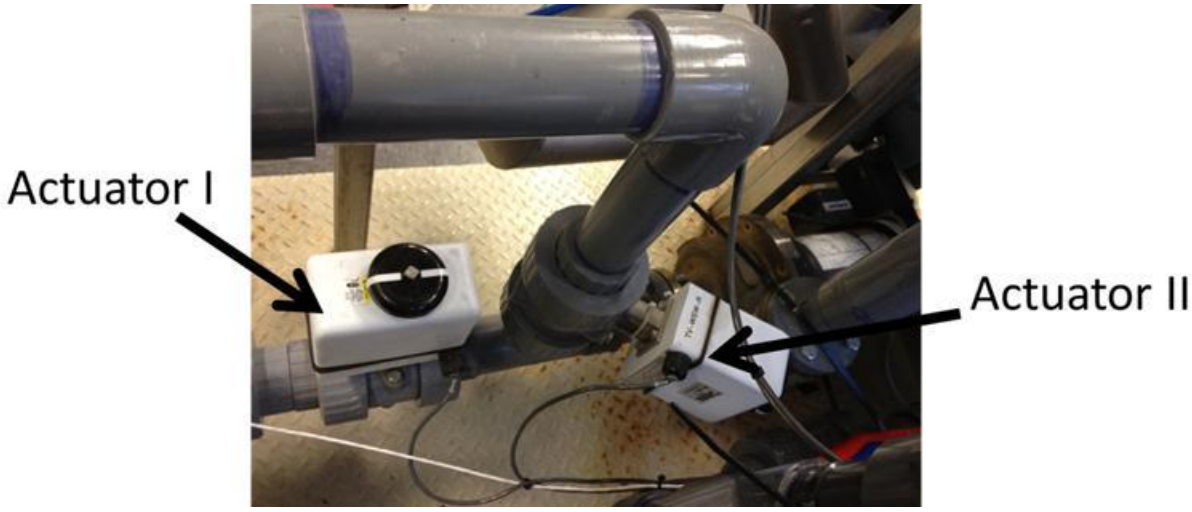

Figure 27: Actuator and valve for water temperature control

As shown in Figure 16, there were two separate water streams feeding warm water into the water pump, one from the warm water storage tank and other from the water return route, and each stream passed through its own actuator. Then by adjusting the opening of both actuators, the two streams mixed in a certain ratio to achieve the desired temperature. The same method was used for the cold water loop to control its inlet water temperature.

A detailed description for all the equipment mentioned above is summarized in Table 2.

Table 2: Equipment specifications

Instrument	Manufacturer	Model	Specification
Refrigerant pump	Hydra·Cell	P400N-SWSS005C	Flow rate: 127 cm^3/s at a pressure of 689 kPa
VFD	Allen-Badley	22B-V5P0N104	Output power: 0.75 kW
Heating tape	BriskHeat	NIH101040L	Electric resistance: 15 Ω
EXV	HANBAY	MCL-000AF	Torque: 0.15 N*m
Chiller	ADVANTAGE	OACS-30S-M1	Cooling capacity: 105.3 kW
Heater	Coates	34854PHS-4	Heating capacity: 54 kW
Actuator	ASSURED AUTOMATION	EV3S3V9T1	Torque: 33.9 N*m
Warm water pump	US MOTORS	F114	Horse power: 2
Cold water pump	US MOTORS	F114	Horse power: 2

2.3 Instrumentation and Data Acquisition (DAQ) system

2.3.1 Measurement instrument

In this study, there were only four types of measurements acquired during testing, namely flow rate, temperature, pressure and power. I measured flow rate for the two water loops mentioned in the previous section, as well as for the refrigerant. I measured the temperatures at the inlet and outlet of all heat exchangers, both for the water side and refrigerant side. I always measured the corresponding pressure at the same point as the temperature, as depicted in Figure 28.

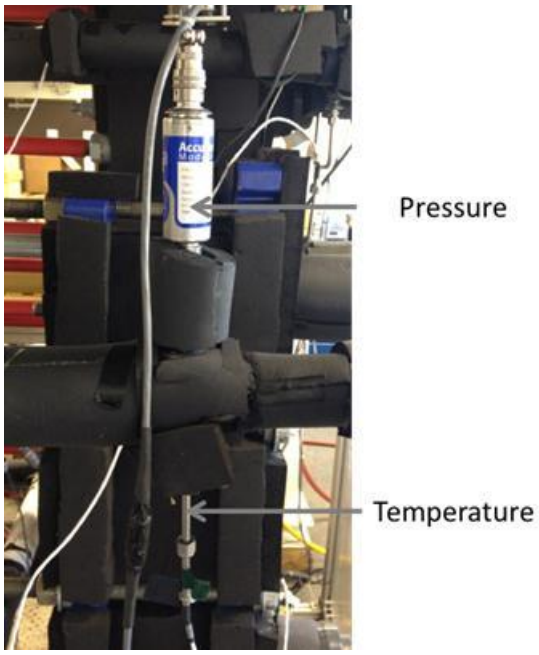

Figure 28: Pressure and temperature measurement point

Heat added by the pre-heating and post-heating tape was the power supplied to the tape, and they were the only power measurements. A detailed description of all measuring instruments is summarized in Table 3.

Table 3: Measuring instrument specifications

Instrument	Measurement Point	Type	Manufacturer	Model	Range	Systematic Uncertainty
Mass/Volume Flow Meter	Condenser cold water	Coriolis	Micro Motion	CMF100H	0 ~ 3.5 kg/s	0.05%
	Evaporator warm water	Coriolis	Micro Motion	CMF100H	0 ~ 3.5 kg/s	0.05%
	Refrigerant	Coriolis	Micro Motion	CMF025H	0 ~ 100g/s	0.05%
Temperature Sensor	All measurement points	Resistance Temperature Detector	Omega	P-M-1/10-1	-100 ~ 400^{o}C	0.03^{o}C
Pressure Sensor	Condenser Refrigerant Inlet	Strain Pressure Transducer	WIKA	S-10	0 ~ 1724 kPa	0.125%
	Condenser Refrigerant Outlet	Strain Pressure Transducer	Setra	ASM1200 PA2M11B 3B00	0 ~ 1379 kPa	0.05%
	Evaporator inlet/outlet	Strain Pressure Transducer	Setra	280E	0 ~ 1724 kPa	0.11%
Power Meter	Pre-heating Tape	Watt Meter	OHIO SEMITRONICS	GH-020D	0 ~ 4000 W	0.2%
	Post-heating Tape	Watt Meter	OHIO SEMITRONICS	PC5-002X5	0 ~ 1000 W	0.5%

2.3.2 Instrumentation

All the instruments listed above were connected to the Data Acquisition (DAQ) modules (Figure 29). Modules used include NI 9203, 9205, 9217, and 9219, each of which reads either current, voltage from every sensor, or specifically for RTD temperature readings, and then converted into actual values for each measurement point.

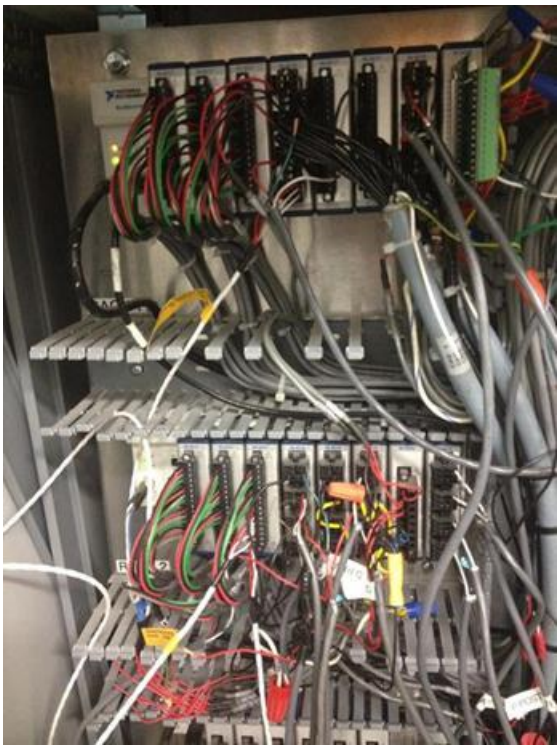

Figure 29: DAQ module

System control was accomplished using a custom program written in LabVIEW interface, as seen in Figure 30. The control was based on proportional- integral-derivative (PID) algorithm. I first entered desired values for each measurement point, and then by reading the current values, LabVIEW adjusted parameters such as pump speed and actuator opening to force the measurement point approach to the set values. The three PID

parameters were adjustable to reduce fluctuation in the measurement data. For every experimental run in this study, after the system had reach steady state, I collected data for the next hour and then process it in the analysis stage.

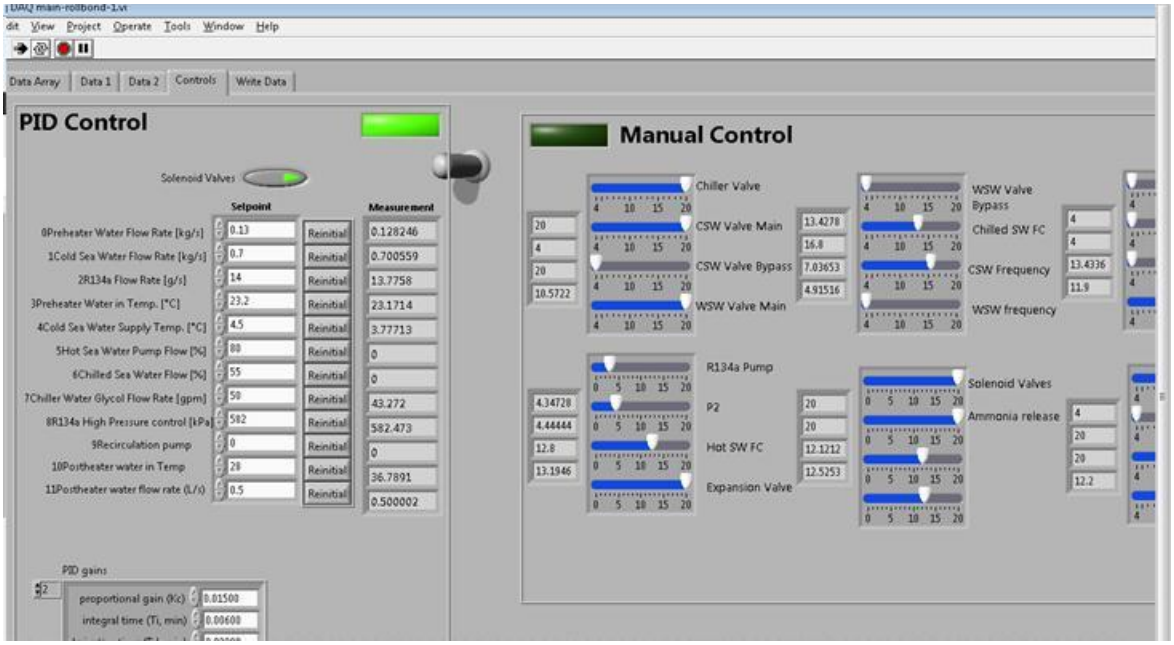

Figure 30: LabVIEW PID control

2.3.3 Instrument calibration

Even though the characteristic curves of all sensors are already given by the manufacturer, I calibrated the mass flow meters and pressure transducers before the first testing. For the mass flow meter, different flow rates of water were ran through the mass flow meter, the process was timed and total water mass was measured, and I obtained water mass flow rate. I then calculated mass flow rate and plotted it against mass flow meter signal output to construct a best-fit straight line. I did pressure transducer calibration in a similar way, except that I used a pressure calibration kit as the reference, which measured the pressure

very accurately. Results for the refrigerant mass flow meter calibration and one of the pressure transducers can be seen in Figure 31 and Figure 32, respectively.

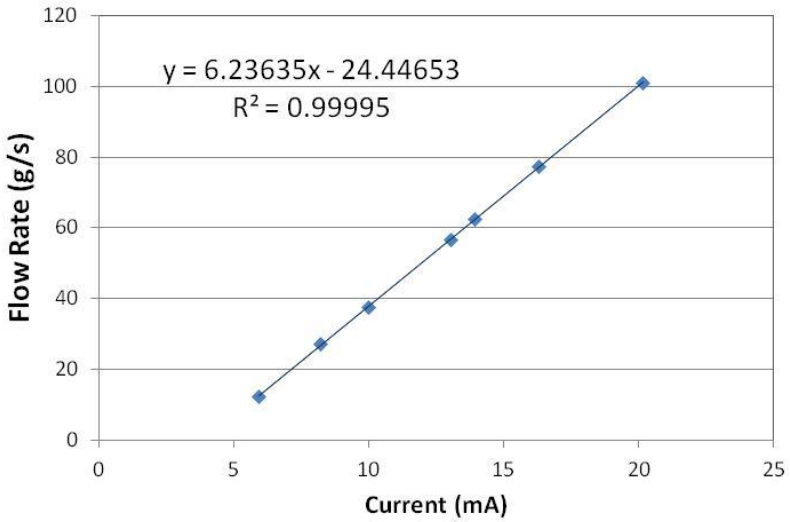

Figure 31: Refrigerant mass flow meter calibration

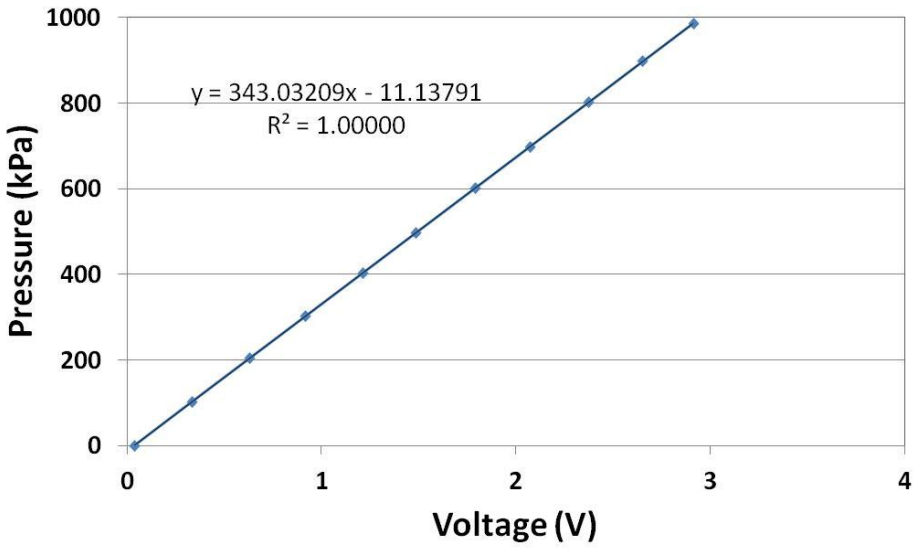

Figure 32: Pressure transducer calibration

2.4 Test procedure

As mentioned previously, the goal of this study is to investigate the effects of evaporation pressure, heat flux, mass flux, and vapor quality on refrigerant-side HTC. The test matrix to achieve this goal is summarized in Table 4.

Table 4: Test matrix for evaporation HTC

Test run set	Refrigerant mass flux G_r (kg/(m^2 s))	Evaporation pressure/temperature P_{sat} (kPa)/T_{sat} (^oC)	Heat flux q_w'' (W/m^2)	Water mass flux G_w (kg/(m2 s))	Quality x
1	1.28	683/25.86	110	12.2	0.15 - 0.95 with 0.1 increment
2	1.28	683/25.86	190	12.2	0.15 -0 .95 with 0.1 increment
3	1.28	533/17.73	110	12.2	0.15 -0 .95 with 0.1 increment
4	1.28	533/17.73	190	12.2	0.15 - 0.95 with 0.1 increment
5	1.70	533/17.73	190	12.2	0.15 - 0.95 with 0.1 increment

As shown in Table 4, due to a large water flow rate required by LTLHP, the evaporator was operated at a low refrigerant mass flux range, and water mass flux was much higher than that of refrigerant.

Before starting the testing, I performed a leakage check for the entire system, including all heat exchangers and piping. Once the system was leak tight, I charged sufficient

amount of refrigerant into the system, until achieving sub-cooling was at the outlet of the condenser, from there I observed a steady refrigerant flow.

When the test facility was ready, and the desired mass flux first established - with condenser running to maintain sub-cooling at its outlet. Then the heat generated by the pre-heating tape was varied by adjusting a transformer that supplied voltage to the tape, and the refrigerant quality entering the evaporator changed according to the heat added to the refrigerant. In order to achieve the required heat flux and evaporation pressure at the same time, I first fixed warm water flow rate to a certain value (0.05 kg/s). Afterward I tuned the inlet water temperature and opening of EXV simultaneously, so that the targeted heat flux was achieved at the specified evaporation pressure. For most of the test runs, refrigerant was still a two-phase mixture coming out of the evaporator, therefore, I controlled the post-heating tape similar to the pre-heating tape, so that superheating was reached before entering the condenser. As a result, evaporation heat transfer at different vapor qualities, evaporation pressures, heat fluxes, and mass fluxes were measured by repeating the above steps.

2.5 Energy balance

Even though heavy insulation was applied to the heat exchangers and connecting piping, heat loss/gain to the ambient was unavoidable, so an energy balance check was performed for every experimental run. For the water side, since RTD was installed at all heat exchanger inlets and outlets, I can calculate water-side heating/cooling capacity based on water mass flow rate, water temperature change and water specific heat at atmospheric pressure according to Eq. 2.1. For the refrigerant side, enthalpy method can

only be used for either superheated or sub-cooled refrigerant, hence only the state points at condenser inlet (superheated vapor) and outlet (sub-cooled liquid) were considered for refrigerant-side capacity, according to Eq. 2.2.

$$\dot{Q}_w = \dot{m}_w * c_{p_w} * (T_{w,i} - T_{w,o}) \quad \text{Eq. 2.1}$$

$$\dot{Q}_r = \dot{m}_r * \Delta h_r \quad \text{Eq. 2.2}$$

Then energy balance is calculated as shown in Eq. 2.3.

$$\epsilon = \left(1 - \frac{\dot{Q}_r}{\dot{Q}_w}\right) * 100\% \quad \text{Eq. 2.3}$$

In addition to the energy balance check of the condenser, evaporator was also checked for energy balance with a fully evaporated run, in which refrigerant entered the evaporator as sub-cooled liquid and exits as superheated vapor. And the same set of equations was used to calculated energy balance of the evaporator. The actual values of energy balance for all tests will be shown in later section of this thesis.

2.6 Uncertainty analysis

For any experiment work, measurement is very important, but accuracy of that number cannot be neglected, and the most common way to determine a measurement's accuracy is uncertainty analysis.

In general, uncertainty in an experimental testing has two components, namely systematic uncertainty and random uncertainty. Systematic uncertainty comes from measurement device itself, as given by the manufacturer, and it is usually a constant or it depends on the measuring range. The associated systematic uncertainty for all measuring instruments can be found in Table 3.

On the other hand, random uncertainty for the measured parameters is the fluctuation between every data recorded during the one-hour period, and a conventional way to calculate random uncertainty is to use the standard deviation. Then total uncertainty is the sum of systematic and random uncertainties.

The above method is only applicable for parameters that are measured directly. For the other parameters such as enthalpy and capacity, which are calculated from other measured parameters, Pythagorean summation of uncertainties is used. To better demonstrate the method, enthalpy is used as an example. In general, enthalpy is a function of both pressure and temperature, and each is associated with its own uncertainty. Using Pythagorean summation, the uncertainty of enthalpy based on temperature and pressure is calculated as in Eq. 2.4.

$$\omega_h = \sqrt{(\frac{\partial h}{\partial P}\omega_P)^2 + (\frac{\partial h}{\partial T}\omega_T)^2} \qquad \text{Eq. 2.4}$$

Instead of direct differentiation of enthalpy with respect to temperature and pressure, approximation using the maximum/minimum values of temperature and pressure and the corresponding enthalpies is made as shown below:

$$\frac{\partial h}{\partial P} = \frac{h(P_{max}) - h(P_{min})}{P_{max} - P_{min}} \quad \text{Eq. 2.5}$$

$$\frac{\partial h}{\partial T} = \frac{h(T_{max}) - h(T_{min})}{T_{max} - T_{min}} \quad \text{Eq. 2.6}$$

Where

$$P_{max/min} = P_{measured} \pm \omega_{P,total} \quad \text{Eq. 2.7}$$

$$T_{max/min} = T_{measured} \pm \omega_{T,total} \quad \text{Eq. 2.8}$$

I calculated uncertainties for the other calculated parameters in similar ways.

Following the above procedure, uncertainties for all parameters can be formulated and a list of typical values for both actual value and uncertainty related to the evaporator can be seen in Table 5.

Table 5: Typical values of uncertainty

	Unit	Measured value	Uncertainty
$T_{w,i}$	^{o}C	20.33	0.02
$T_{w,o}$	^{o}C	18.80	0.08
$\dot{m}_w$	kg/s	0.05	0.00
$\dot{Q}_w$	W	320	20
$\dot{Q}_{t\_post}$	W	517	30
$T_{r,evap,i}$	^{o}C	19.29	0.06
$P_{r,evap,i}$	kPa	537.88	2.90
$T_{r,evap,i,sat}$	^{o}C	18.04	0.17
$h_{r,evap,i}$	kJ/kg	270.47	4.14
$x_{r,evap,i}$	-	0.25	0.02
$T_{r,evap,o}$	^{o}C	18.27	0.07
$P_{r,evap,o}$	kPa	528.40	2.95
$T_{r,evap,o,sat}$	^{o}C	17.48	0.18
$h_{r,evap,o}$	kJ/kg	323.77	4.96
$x_{r,evap,o}$	-	0.54	0.18
$h_{r,evap,avg}$	kJ/kg	297.12	3.23
$P_{r,evap,avg}$	kPa	533.14	2.07
$T_{r,evap,sat}$	^{o}C	17.76	0.12
$x_{r,evap,avg}$	-	0.40	0.02
$LMTD_{r,evap}$	K	1.69	0.14
U_{evap}	W/m^2*K	109	11
$h_{w,evap}$	W/m^2*K	402	-
$h_{r,evap}$	W/m^2*K	207	11
G_r	kg/m^2*s	1.28	0.00
q_w''	W/m^2	184	10

2.7 Data reduction

As mentioned in the previous section, I varied evaporator inlet quality by changing the heat inputs from the pre-heating tape. Instead of using the heat of pre-heating tape directly, evaporator outlet enthalpy was first evaluated using the superheated vapor state after the post-heating tape and post-heating tape power, as shown in Eq. 2.9 and Eq. 2.10.

$$h_{evap,o} = h_{cond,i} - \frac{\dot{Q}_{t\_post}}{\dot{m}_r} \quad \text{Eq. 2.9}$$

$$h_{evap,i} = h_{evap,o} - \frac{\dot{Q}_w}{\dot{m}_r} \quad \text{Eq. 2.10}$$

At the end, evaporator quality was found using refrigerant property, as shown in Eq. 2.11.

$$x_{evap,m} = x\left(\frac{h_{evap,o} + h_{evap,i}}{2}, P_{evap,m}\right) \quad \text{Eq. 2.11}$$

For the overall HTC, logarithmic mean temperature difference (LMTD) is used. In general, LMTD is used for single phase heat transfer, where temperature gradient is assumed to be constant along the heat exchanger. However, in this study, evaporation is taking place, and the temperature of the refrigerant is the evaporation temperature at the corresponding pressure. Since there is pressure drop from inlet to outlet of the evaporator, outlet temperature of the refrigerant is lower than inlet temperature, making the regular LMTD method not applicable, and modification has to be made. Several researchers (Han, 2003 and Wellsandt, 2003) had suggested the same idea, which used the average

evaporation temperature based on the average evaporation pressure, instead of the refrigerant inlet and outlet temperatures (Eq. 2.12), and it can better reflect the temperature profile.

$$\mathrm{LMTD} = \frac{\mathrm{T_{w,i}} - \mathrm{T_{w,o}}}{\ln\left(\frac{\mathrm{T_{w,i}} - \mathrm{T_{r,evap,sat}}}{\mathrm{T_{w,o}} - \mathrm{T_{r,evap,sat}}}\right)} \qquad \text{Eq. 2.12}$$

Regarding the heat transfer area, nominal area of the plate is used, which is given by the manufacturer and can be seen in Table 1.

At last, total heat transfer is needed to calculate the overall HTC. Since refrigerant is a two-phase mixture at the inlet and outlet of the evaporator, heat transfer inside the evaporator was calculated based on the water side measurement. In this case, evaporator heat capacity was found using water mass flow rate, water inlet and outlet temperature, as shown in Eq. 2.13, where c_{pw} is evaluated at atmospheric pressure.

$$\dot{\mathrm{Q}}_{\mathrm{w}} = \dot{\mathrm{m}}_{\mathrm{w}} * \mathrm{c_{p_w}} * (\mathrm{T_{w,i}} - \mathrm{T_{w,o}}) \qquad \text{Eq. 2.13}$$

Then overall HTC is calculated as:

$$\mathrm{U} = \dot{\mathrm{Q}}_{\mathrm{w}}/(\mathrm{A_{total}} * \mathrm{LMTD}) \qquad \text{Eq. 2.14}$$

2.8 Water-to-water test

As shown in the previous section, overall HTC can be calculated using the LMTD method, but in order to determine the refrigerant side heat transfer, water side HTC has to be known. This is better explained with thermal resistance as in Eq. 2.15 and Eq. 2.16:

$$R_{ov} = 1/(U * A_{total}) \quad \text{Eq. 2.15}$$

$$R_{ov} = R_r + R_{wall} + R_w \quad \text{Eq. 2.16}$$

Due to the small thickness of the plate, thermal resistance of the plate wall was neglected, as it was done by researchers like Han (2003). Then in order to evaluate the water side HTC, a modified Wilson plot method was used. According to Fernandez-Seara et al. (2007), the original Wilson plot was first developed to determine convection coefficient in shell-and-tube condenser, and it was based on the concept of thermal resistance. Wilson theorized that if mass flow of only one fluid is changed, the change in overall thermal resistance is mainly related to that fluid, and the other resistance constituents remain unchanged. Then the effect of changing warm water mass flow rate on thermal resistance is based on the assumption that thermal resistance of the warm water side is proportion to $1/v^n$, where n is an exponent obtained from straight line best fitting, and the overall thermal resistance is also a linear function of $1/v^n$. At the end, a plot of $R_{overall}$ vs. $1/v^n$ is drawn and water side thermal resistance can be calculated using the slope m of the best fit straight line:

$$h_w = \frac{1}{m * A_{total}} * v^n \quad \text{Eq. 2.17}$$

As mentioned above, in the original Wilson plot method an assumption was made that cold water side heat transfer is constant when warm water mass flow rate is varied. To account for any change in cold water side heat transfers, a modified Wilson plot method

was generated which also considered variable fluid property effect. According to Khan et al. (2010), for single phase heat transfer, Nu is generally represented as

$$\mathrm{Nu} = \mathrm{C} * \mathrm{Re}^{\mathrm{n}} * \mathrm{Pr}^{1/3} \qquad \text{Eq. 2.18}$$

Also Nusselt number and water side HTC is correlated as:

$$\mathrm{h_w} = \mathrm{Nu} * \frac{\kappa_w}{d_e} \qquad \text{Eq. 2.19}$$

Where C and n only depend on the heat exchanger geometry and are independent of the fluid used. By applying Eq. 2.18, Longo (2010) in his study, instead of plotting $R_{overall}$ and v^n, a modification was made to the X and Y axis as shown in Eq. 2.20 and Eq. 2.21:

$$\mathrm{X} = \frac{\kappa_c}{\kappa_w} * \left(\frac{\mathrm{Re_c}}{\mathrm{Re_w}}\right)^{\mathrm{n}} * \left(\frac{\mathrm{Pr_c}}{\mathrm{Pr_w}}\right)^{1/3} \qquad \text{Eq. 2.20}$$

$$\mathrm{Y} = \left(\mathrm{R_{overall}} - \frac{\mathrm{t}}{\kappa_w}\right) * \frac{\kappa_c}{d_e} * \mathrm{Re_c^n} * \mathrm{Pr_c^{1/3}} \qquad \text{Eq. 2.21}$$

Then by employing a best-fit straight line, slope of the line is equivalent to 1/C in Eq. 2.18.

Once Eq. 2.18 is obtained, warm water side HTC is simply:

$$\mathrm{h_w} = \frac{\kappa_w}{d_e} * \frac{1}{\mathrm{m}} * \mathrm{Re_w^n} * \mathrm{Pr_w^{1/3}} \qquad \text{Eq. 2.22}$$

Chapter 3. Results and Analysis

3.1 Water-to-water test

As shown in the previous section, the modified Wilson plot method requires fluid properties like conductivity, viscosity, specific heat and density. Since fluid property changes with temperature change, I evaluated all properties at the average fluid temperature, as it was done by others like Yan (1999) and Hsieh (2003). For the total heat transfer between cold and hot water stream, I used the average of cold and hot water-side heat transfer, and heat transfer area was assumed to be the same.

Then I followed the test matrix listed in Table 6 to run the water-to-water test, and the range of warm water flow rate was determined based on the test matrix in Table 4.

Table 6: Test matrix for water-to-water test

Warm water flow rate (kg/s)	Warm water-inlet temperature (^{o}C)	Cold water flow rate (kg/s)	Cold water-inlet temperature (^{o}C)	Test run
0.03 to 0.07 with 0.005 increment	35.5	0.1	6	9

A plot based on Eq. 2.20 and Eq. 2.21 was made, which can be seen in Figure 33.

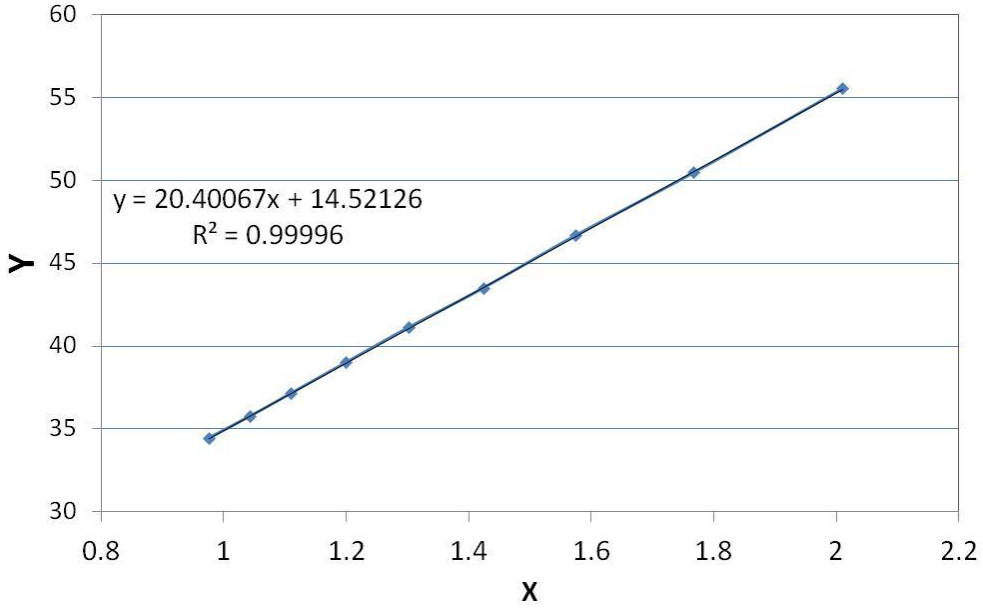

Figure 33: Modified Wilson plot

Based on the best-fit straight line equation in Figure 33, constant C and exponent n in Eq. 2.18 was found to be 0.0492 and 0.85, respectively, and Nu is given as:

$$\mathrm{Nu} = 0.0492 * \mathrm{Re}_{\mathrm{w}}^{0.85} * \mathrm{Pr}_{\mathrm{w}}^{1/3} \qquad \text{Eq. 2.23}$$

With Eq. 2.23, warm-water side HTC in relation to water mass flow can be calculated. Water-to-water test has also been implemented by researchers like Hsieh (2003) and Yan (1999). In their work, they tested the PHE with chevron angle of 30^{o}, which is the same as the present study. However, the plate length (0.45m) and width (0.12m) were smaller than the ones in this study, and their correlations are compared to the current findings, as depicted in Figure 34.

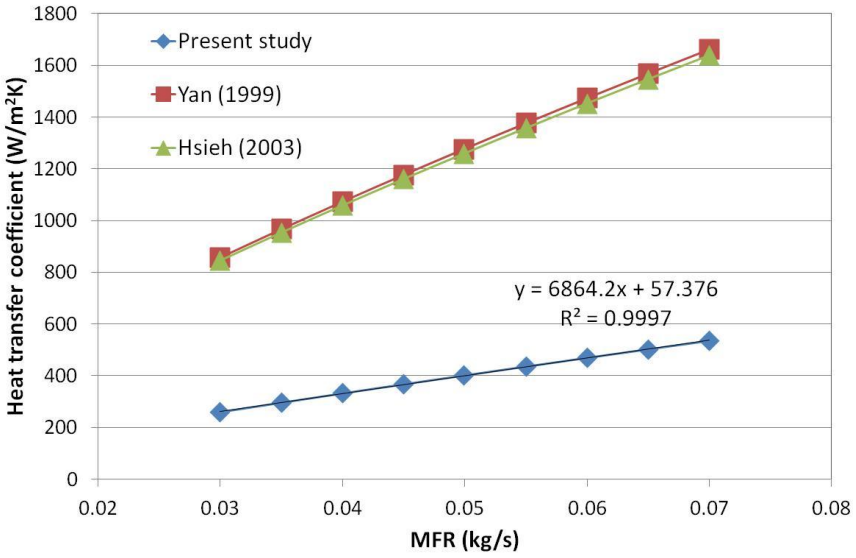

Figure 34: Warm water-side HTC

As shown in Figure 34, the present study shows a lower HTC than the two given correlations, and the difference is probably due to a larger area plate used in this study, leading to a lower water flow velocity at the same mass flow rate. The possible difference in turbulence level is indicated by the difference in Re used between present study and work conducted by Hsieh. Based on the similar results from Yan and Hsieh, the ranges of Re in their studies should be very close to each other. Nevertheless, based on the result and at the operating warm water flow rate of 0.05 kg/s, water-side HTC is interpolated to be 402 W/m^{2}K.

Table 7: Water-to-water test comparisons

	Present study	Yan (1999)	Hsieh (1999)
Plate length (m)	0.65	0.45	0.45
Plate width (m)	0.21	0.12	0.12
Warm water-side Re	34 to 80	Not given	360 to 2250

3.2 Energy balance

As discussed in the previous section, it is always important and necessary to check the energy balance for the system. And because of the limitation of enthalpy method, energy balance was first performed from the condenser inlet (superheated vapor) to condenser outlet (sub-cooled liquid), considering cold-water side and refrigerant-side heat transfer. In addition, the total heat added, which includes pre-heating and post-heating tapes, and evaporator warm water is checked against condenser cold water heat transfer, as well as refrigerant-side heat gain from before pre-heating tape to after post-heating tape, which was the same as condenser side refrigerant heat transfer. Typical energy balance in terms of the system is summarized in Table 8.

Table 8: Energy balance of the system

Condenser water-side (W)	1,162
Condenser refrigerant-side (W)	1,220
Total heat added (W)	1,204
Condenser energy balance (%)	4.95
Refrigerant and heating energy balance (%)	1.27

As shown in Table 8, energy balance of the system is acceptable, as it is less than 5%.

Then a test run with complete evaporation was carried out to test the evaporator energy balance, and the result can be seen in Table 9.

Table 9: Energy balance of evaporator

Refrigerant mass flow rate (g/s)	8.00
Refrigerant inlet sub-cooling (K)	0.91
Refrigerant outlet superheat (K)	1.05
Refrigerant side heat transfer (W)	1,488
Warm water heat transfer (W)	1,521
Evaporator energy balance (%)	2.19

As indicated in Table 9, evaporator energy balance is less than 3%, so the evaporator is also well insulated and heat loss is minimal.

3.3 Two-phase evaporation heat transfer

As mentioned in section 2.4 Test Procedure, the objective of this test is to investigate the effect of mass flux, evaporation pressure, heat flux, and vapor quality on the two-phase evaporation heat transfer. Based on the energy balance check I carried out, the overall heat transfer matched with water-side heat transfer, which can be calculated based on water-side temperatures and water mass flow rate measurements. Once overall HTC or the total thermal resistance is computed, refrigerant-side thermal resistance is determined by subtracting the water-side thermal resistance, which I found from water-to-water test. At the end, the refrigerant evaporation HTC is calculated accordingly.

3.3.1 Heat flux

I maintained mass flux maintained constant at 1.28 kg/m^{2}s, with a varied vapor quality. Figure 35 and Figure 36 show the effect of heat flux on HTC at two different evaporation pressures (683 kPa and 533 kPa), respectively. At both evaporation pressures, evaporation HTC is higher when heat flux is higher, and then both HTCs drop significantly as quality approaches one. In general, an increase in evaporation HTC with heat flux is an indication of nucleate boiling, which is a region defined in pool boiling (ASHRAE, 2005). During nucleate boiling, superheated liquid forms a thin layer on the heating surface, and bubbles nucleate and then grow from spots on the surface. Heat transfer is enhanced by bubble-induced movement and vaporization. One measure that is very important for nucleate boiling is the difference between wall temperature and liquid saturation temperature, which is also called excess temperature. And this temperature difference is directly related to heat flux. As the excess temperature increases, bubble formation is intensified, and there is a rise in both HTC and heat flux across the heat transfer surface. As excess temperature increases further (around 10^{o}C), HTC reaches its maximum as high concentration of vapor inhibits liquid motion near the surface (Incropera, 2007), but heat flux keeps increasing due to larger excess temperature. Eventually heat flux also reaches to a maximum point when large number of vapor prevents the liquid to continuously wet the surface, and critical heat flux is defined at this point. Since the excess temperature in the present study is very small (1.3 – 2.3^{o}C), an increase in excess temperature not only aids bubble formation, but also causes an increase in HTC, as well as heat flux.

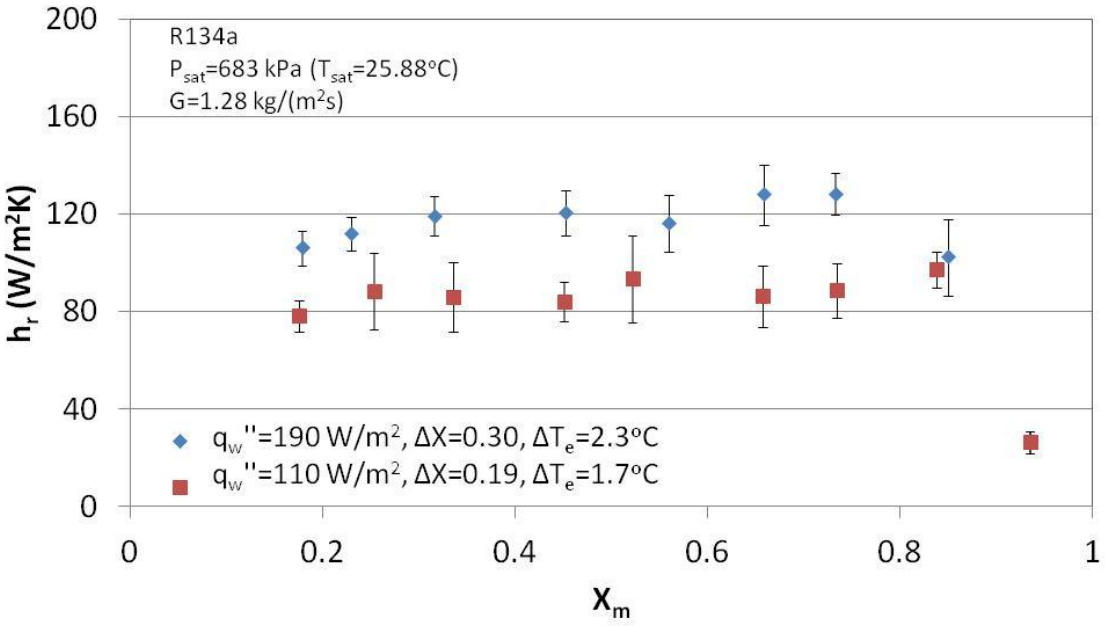

Figure 35: Evaporation HTC vs. vapor quality, at P_{sat}=683 kPa and G=1.28 kg/m^{2}s

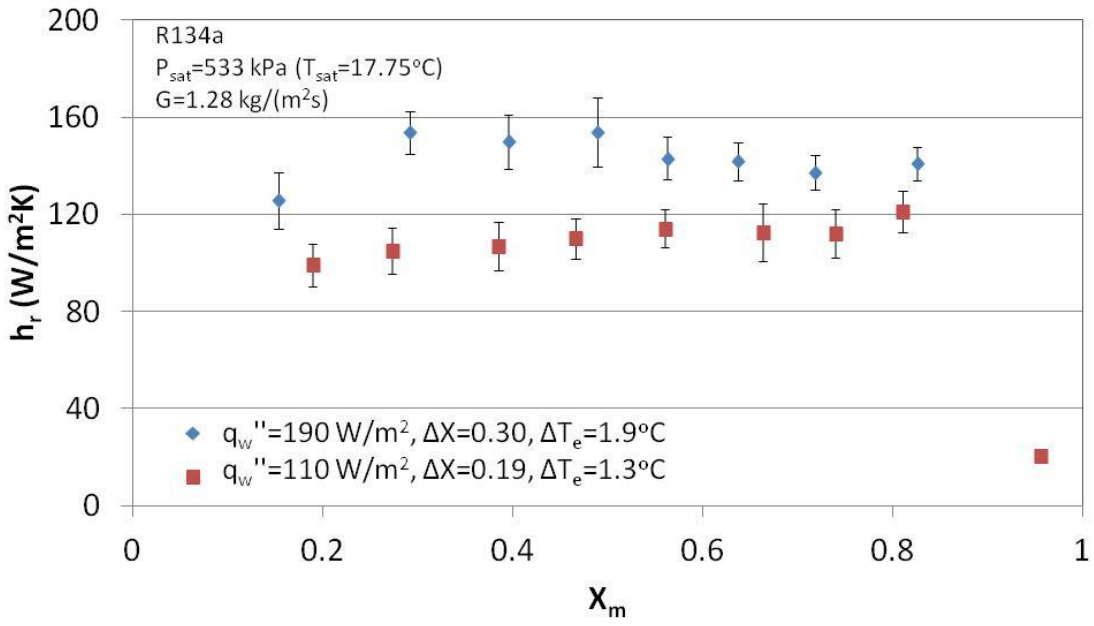

Figure 36: Evaporation HTC vs. vapor quality, at P_{sat}=533 kPa and G=1.28 kg/m^{2}s

When referring back to Figure 35 and Figure 36, you will see that when heat flux is higher, excess temperature is also higher accordingly at both saturation pressure levels,

and a higher HTC indicates the presence of nucleate boiling. In addition, when saturation pressure changes from 683 kPa to 533 kPa, excess temperature decreases at the same heat flux level, which means bubble is easier to form at a lower pressure.

In terms of vapor quality, as it increases, the change in evaporation HTC is not significant, which is different from testing done by Han et al. (2003). In their study, evaporation heat transfer of R410A inside a BPHE was found to improve with vapor quality. As they explained, specific volume of refrigerant vapor is much larger than liquid, and for the same mass flux, specific volume increases with vapor quality, so refrigerant flow becomes much faster for a higher vapor quality region. As this happens, the evaporation process is in forced convection dominant boiling. During forced convection boiling, flow is due to bulk motion of the fluid, as well as to buoyancy effects (Incropera, 2007). As the flow velocity increases, fluid motion on the heat transfer surface is intensified, leading to an increase in HTC. Due to strong turbulence inside PHE, they concluded that the evaporation heat transfer was still at convective mode even at low quality and low mass flux, and effect of nucleate boiling was reduced.

On the other hand, in the study done by Yan et al. (1999), R134a was used for PHE evaporation heat transfer testing. And similar to Han's (2003) results, they observed an increase in HTC with vapor quality. The effect of vapor quality was most significant when the vapor quality is higher than 0.45, and the evaporation HTC increased almost exponentially with quality. Unlike vapor quality, heat flux had very little impact on HTC, except at the low-vapor quality, where nucleate boiling was more dominant than convection boiling.

In the current study, the effect of vapor quality on HTC is insignificant except for the point with highest vapor quality, where dry out is likely to occur. Dry out was also observed in the study conducted by Longo (2010), where he found a much smaller evaporation HTC as outlet quality became high for R134a test inside a BPHE evaporator. He also pointed out, when dry out occurs, heat is transferred mostly through the single phase vapor, and the single phase HTC is one or two order of magnitude lower than two phase heat transfer.

In conclusion, the lesser impact of vapor quality on heat transfer indicates nucleate boiling is the dominant mode over convective boiling in this study. This is confirmed by a much smaller refrigerant mass flux of 1.28 kg/m^{2}s in this study, compared to 27 kg/m^{2}s of R410A used by Han (2003) and 70 kg/m^{2}s of R134a used by Yan (1999). Again, the small R134a mass flux is due to the low refrigerant mass flux required by LTLHP, which is different from tests done by other researchers. Moreover, the primary reason for using such a low refrigerant mass flux was that, pre-heating and post-heating capacity from the heating tape (Figure 18) were both limited, and only by introducing low refrigerant flow rate, vapor quality could be controlled to vary between 0.15 and 0.95.

3.3.2 Evaporation pressure

While the evaporation pressure was varied, the evaporation HTC was measured at two different heat fluxes levels. The results are displayed in Figure 37 and Figure 38.

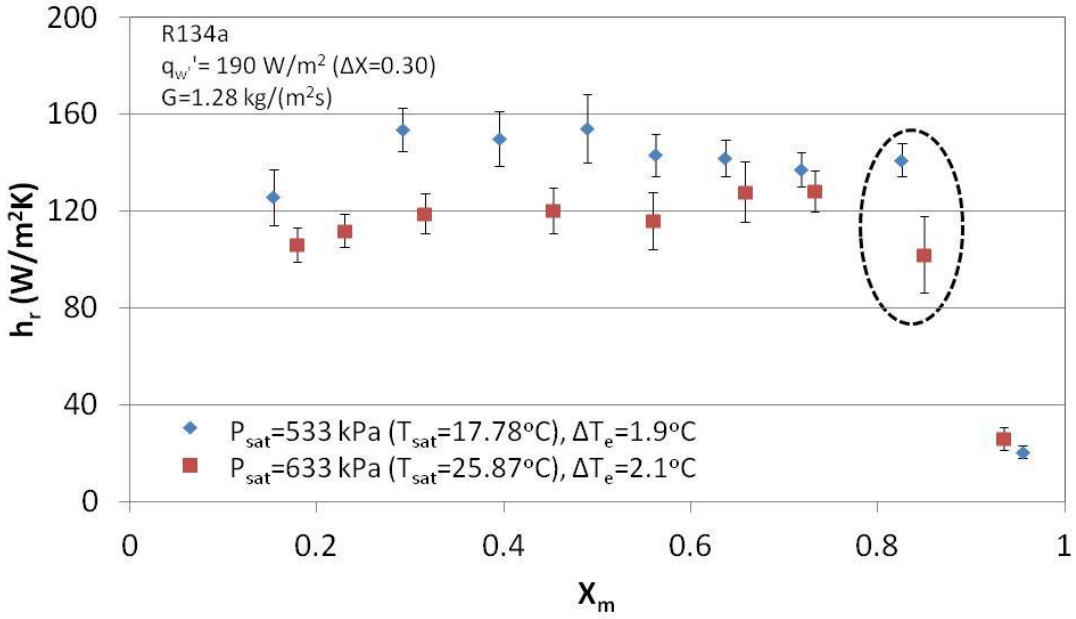

Figure 37: Evaporation HTC vs. vapor quality, at q_w''=190 W/m^2 and G=1.28 kg/m^{2}s

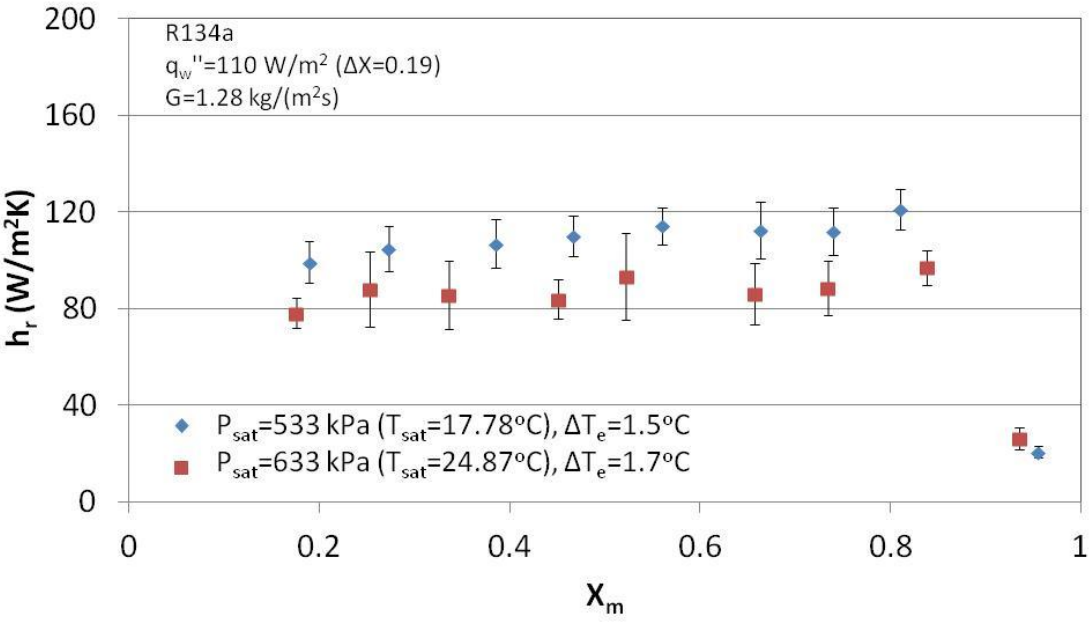

Figure 38: Evaporation HTC vs. vapor quality, at q_w''=110 W/m^2 and G=1.28 kg/m^{2}s

As shown in Figure 37 and Figure 38, overall, evaporation heat transfer is better for lower saturation pressure, but the effect is not significant, especially for the higher heat

flux case. For that case (Figure 37), when vapor quality is high, the difference between HTCs for the two evaporation pressures tested is not uniform. Instead, for the lower heat flux test run (Figure 38), the difference is more even throughout the vapor quality domain. The slight increase in evaporation HTC with decreasing evaporation pressure can be explained with excess temperature. When the evaporation pressure decreases, excess temperature also decreases for the two different heat fluxes used. This observation confirms with the previous conclusion that a lower evaporation pressure leads to easier bubble formation. When there is more bubble leaving the surface, fluid movement is enhanced, and a better evaporation HTC is obtained, which in turn requires a smaller excess temperature to achieve the same heat flux.

The effect of evaporation pressure on evaporative heat transfer was also discussed by Sun et al. (2007), where they measured HTCs of nucleate boiling on a smooth flat surface for pure R134a. In their study, they found that the HTC increased with evaporation pressure for the nucleate boiling, and they explained that this was due to change in thermodynamic properties of refrigerant such as a reduced bubble formation power, which could enhance evaporation heat transfer. This is in contrary to the trend seen in this study, where a lower evaporation pressure causes bubble to form more easily, and providing better heat transfer. Such contradiction is probably due to a different excess temperature and heat flux provided. Throughout this study, a smaller heat flux of 190 W/m^2 was used, compared to a heat flux more than 300,000 W/m^2 used by Sun. When excess temperature and heat flux (190 W/m^2) are low like in the present study, bubble formation only induces fluid motion near the surface and improves evaporation heat transfer. However, when heat flux is much higher like in Sun's study, and a stronger bubble formation may

interfere with fluid motion near the heat exchange surface and evaporation HTC could be reduced.

If evaporation is under convective boiling region, a positive effect of decreasing evaporation pressure on evaporation HTC can be observed, as discussed by both Han (2003) and Yan (1999). In the two studies, they detected an improvement in heat transfer with decreasing evaporation pressure, especially for the higher quality region. Plus, they attributed the improvement to a higher specific volume for a lower evaporation process, hence enhancing the convective boiling. When vapor quality was low, the effect of saturation pressure on heat transfer was small, and it was probably due to the dominance of nucleate boiling over convective boiling. Yan (1999) also pointed out latent heat of vaporization is smaller for a higher evaporation pressure, and the channel wall may be partially dried out when vapor quality is high for the higher evaporation pressure. In his testing, evaporation pressure of 675 kPa and 800 kPa were used for R134a, and their respective heat of vaporization was 177.4 kJ/kg and 171.9 kJ/kg, so there was a difference of 5.5 kJ/kg. For the present study, with evaporation pressure of 533 kPa and 683 kPa, the difference in heat of vaporization is 7.3 kJ/kg. The difference in heat of vaporization difference could be the cause of a sudden enlargement in HTC difference between the two pressure levels at the same vapor quality, as enclosed by the dashed line in Figure 37. The heat transfer surface encounters a more severe drying-out for the higher evaporation pressure test point.

In conclusion, a higher evaporation HTC is obtained with lower evaporation pressure, which is a characteristic in convective boiling. However, the lack of influence from vapor

quality shows convective boiling is not dominant, and the improvement in evaporative heat transfer from reduced evaporation pressure is due to more favorable vapor formation, as well as better fluid motion near the heat exchange surface.

3.3.3 Mass flux

Lastly, evaporation heat transfer at two different mass fluxes at the same heat flux level and evaporation pressure was tested and compared, and the result can be seen in Figure 39.

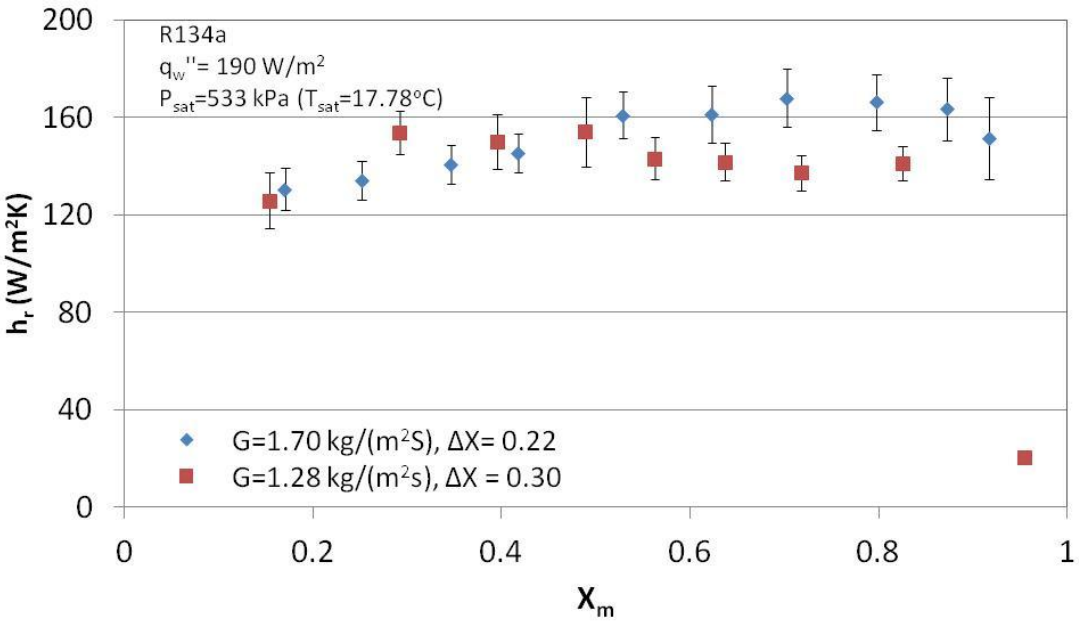

Figure 39: HTC vs. vapor quality, at q_w''=190 W/m^2 and P_{sat}=533 kPa

As displayed in Figure 39, even though heat flux for both cases is the same, due to a different mass flux, quality change within the evaporator is higher for the lower mass flux case. Also the effect of mass flux on HTC is insignificant at low quality region, and becoming more obvious once quality is higher than 0.5, indicating convective heat

transfer has larger influence when vapor quality is high. Han (2003) and Yan (1999) also found positive effect of mass flux on evaporation heat transfer. And similar to current findings, results for R134a by Yan showed insignificant influence of mass flux at low vapor quality, and he pointed out boiling in the refrigerant at low vapor quality appeared to be suppressed. Then once quality became higher, difference in HTC for the two mass fluxes (70 kg/m^{2}s and 55 kg/m^{2}s) tested started to grow, with higher mass flux increasing more quickly with quality. Again, the increase in evaporation HTC was explained with a much higher specific volume of vapor than liquid, and refrigerant flows in a much higher speed when vapor quality is higher, which helps to break liquid film on the heat transfer surface and enhance heat transfer.

Based on the mass flux comparison study, it can be shown that convective boiling is present in the current study, but only limited to high vapor quality region.

3.4 Conclusions

In summary, low refrigerant mass flux conditions as required for LTLHP application in the current study seems to suppress the influence of convective boiling, and this is evident from the insignificant effect of vapor quality on evaporative HTC. However, when heat flux increased, evaporative HTC also increased, and it is an indication of nucleate boiling. Excess temperature was also studied, which relates closely to nucleate boiling regime. As evaporation pressure decreased, it became easier for vapor bubble to generate when pressure was lower, indicated by a lower excess temperature. And a more rigorous bubble movement at a low excess temperature range involved in this study enhanced heat transfer across the surface, and evaporative HTC increases. At last, when

the mass flux is increased, evaporative HTC increased accordingly, indicating that convective boiling was present, and it just played a smaller role in the evaporation heat transfer because of a slow fluid flow.

Chapter 4. Cycle Simulation

4.1 Introduction

In this section, an ASHP and WSHP are simulated and compared in terms of performance and energy consumption in the heating season, based on the temperature data for Nagasaki, Japan from the year of 2000 to 2001, as given in Figure 4 by Song (2007). The comparison is made for the months when outdoor temperature is below 20^{o}C and heating is assumed to be required. The temperature data input is summarized in Table 10.

Table 10: Temperature profiles of ASHP and WSHP in Nagasaki, Japan, 2000 - 2001

Month, year	Outdoor air temperature (^{o}C)	Seawater temperature (^{o}C)
April, 2000	15.3	16.6
November, 2000	15.7	21.7
December, 2000	11.1	18.2
January, 2001	8.5	14.9
February, 2001	9.4	14.6
March, 2001	12.6	15.1
April, 2001	15.5	16.6
November, 2001	14.5	21.8
December, 2001	10.6	17.6

The two systems simulated are simple VCC cycles, and their working fluids are both R134a. Due to the difference in heat source medium, there is small difference between the two systems, and it is better depicted in Figure 40 and Figure 41.

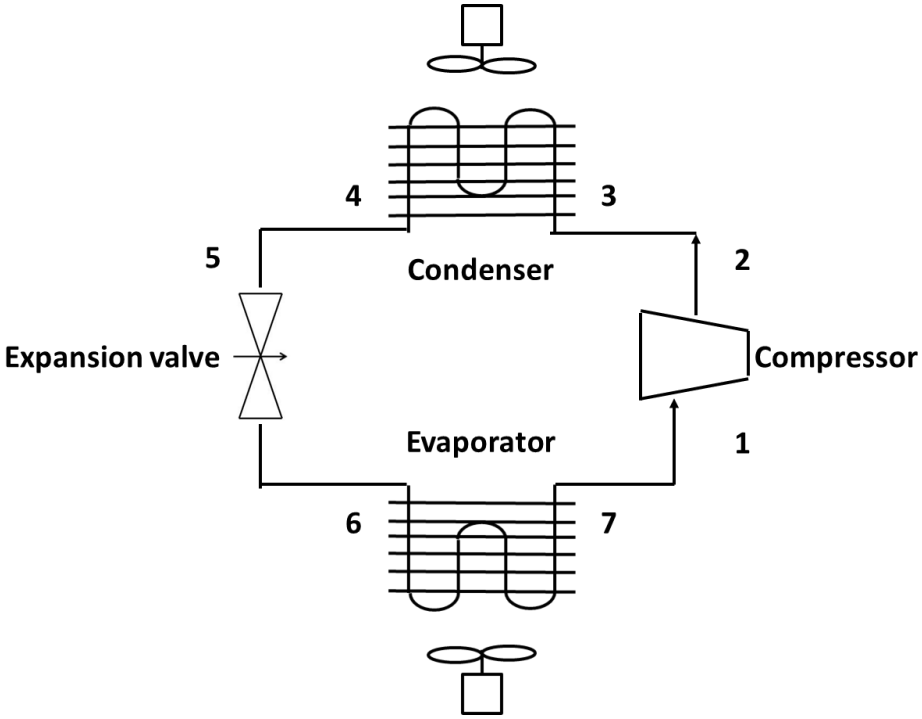

Figure 40: Schematic diagram of ASHP

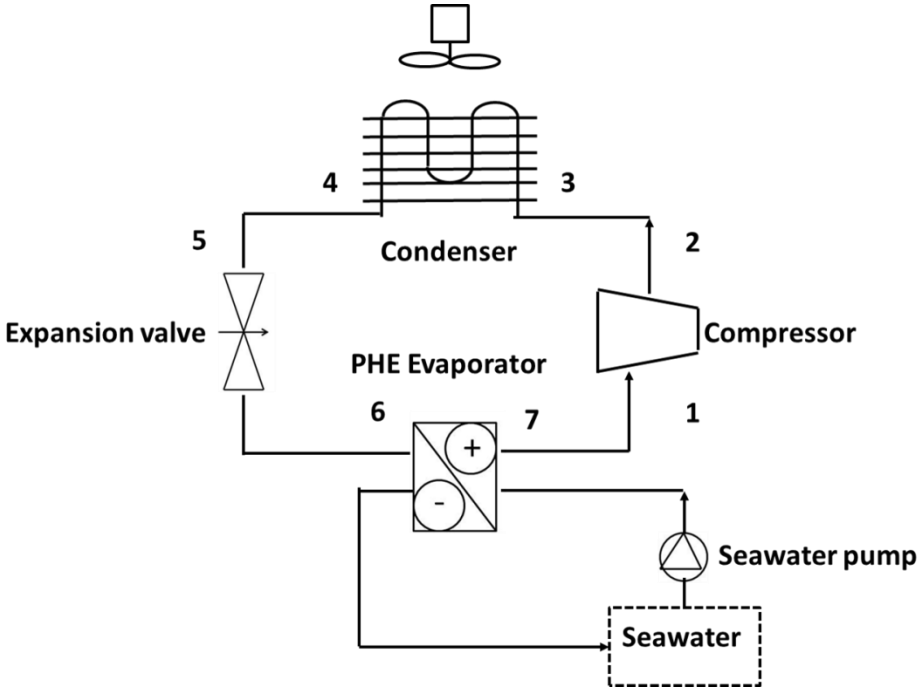

Figure 41: Schematic diagram of WSHP

As shown in the schematic diagrams, for ASHP an air to refrigerant evaporator is used, and an evaporator fan is needed. On the other hand, for WSHP a PHE evaporator is used, and a seawater pump draws seawater into the PHE evaporator through an open-loop configuration, and at the end discharges water directly back into the sea.

4.2 Operating conditions

For both systems, a space temperature is set to 21^{o}C and relative humidity (RH) is 50 percent. Heating capacity is fixed at 1 MW for the nine months duration tested, and all the components except for the evaporator are the same for both systems simulated. Then for ASHP evaporator, heat is transferred from ambient air to the refrigerant, and for WSHP heat is transferred from seawater. Pressure drop in the condenser is assumed to be zero for simplicity, while degree of subcooling at point 5 is maintained at 5K and saturation liquid temperature (point 4) is set to be 10K warmer than space temperature. For the evaporator, a superheating (point 1) of 2K is used, and pressure drop is set to be 10 kPa for both cases. For ASHP, temperature difference between the ambient air and evaporator inlet (point 6) is set to 5K. Due to higher efficiency of WSHP PHE evaporator, seawater outlet is assumed to be 2.5K warmer than evaporator inlet, and temperature change of seawater across the evaporator is allowed to be 2K. A summary of design condition can be seen in Table 11.

Table 11: Design condition

	Parameter	Value
Space	Temperature (^{o}C)	21
	RH (%)	50
Compressor	Isentropic efficiency	0.9 – 0.0467*PR
	Volumetric efficiency	1 – 0.04*PR
	Motor efficiency (%)	95
Condenser fan	Airflow rate (m^3/s*kW)	0.064
	Power input (W/(m^3/s))	180
Evaporator fan	Airflow rate ((m^3/s)/kW)	0.054
	Power input (W/(m^3/s))	775
Water pump	Pump efficiency	0.5

4.3 Simulation results

Since the evaporator performance is of primary interest in this thesis, and the ASHP and WSHP systems simulated are assumed to use the same type of condenser to provide heating, so heating capacity is fixed at 1 MW. Based on the temperatures shown in Figure 42, the two systems are simulated, and the results of evaporator capacity, total work consumption and COP can be seen in Figure 43, Figure 44, and Figure 45. As shown in the comparison graphs, because seawater temperature is higher than ambient air, for the same heating capacity, WSHP requires smaller energy consumption, and it has a higher COP for the heating season than ASHP.

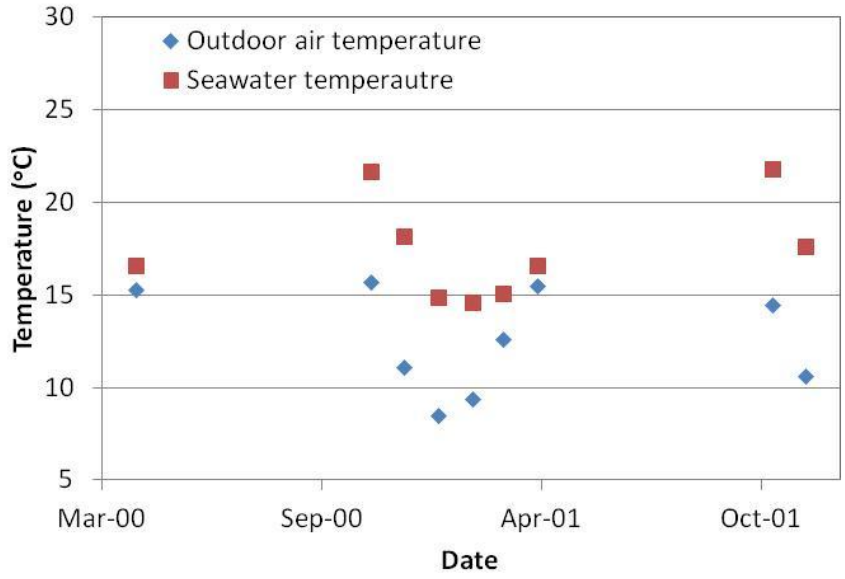

Figure 42: Temperature profiles of ASHP and WSHP in Nagasaki, Japan (Song, 2007)

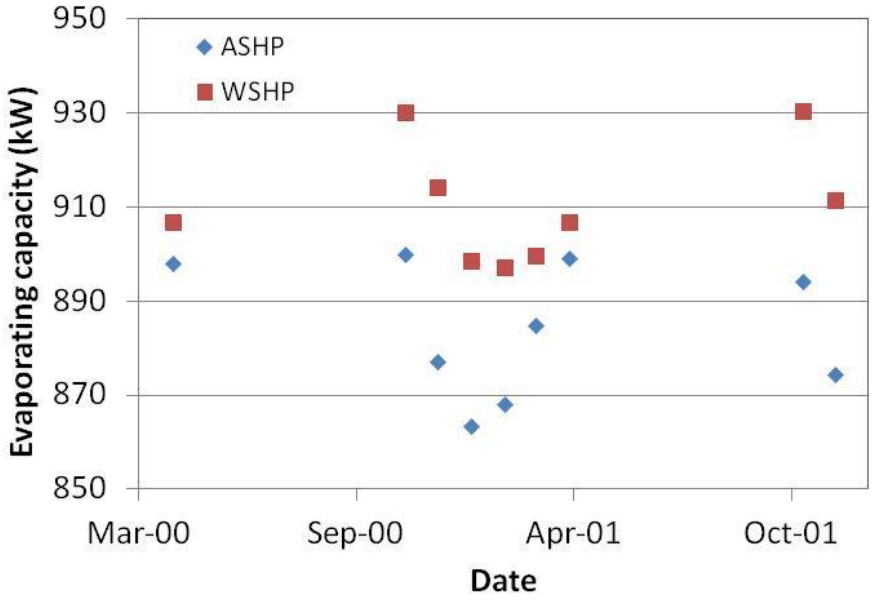

Figure 43: Evaporator capacities of ASHP and WSHP

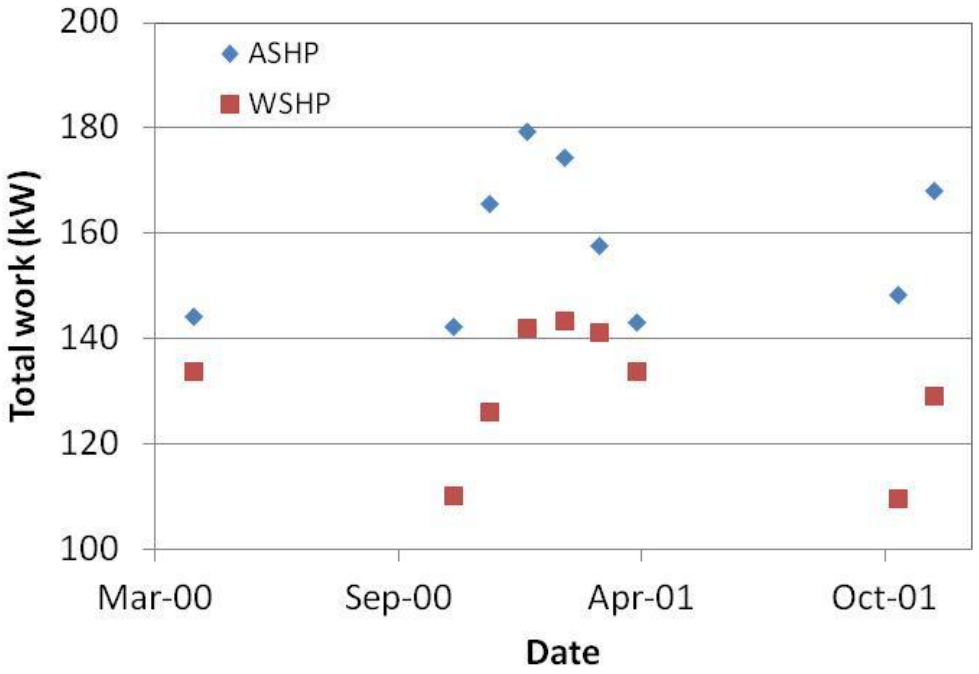

Figure 44: Total energy consumptions of ASHP and WSHP

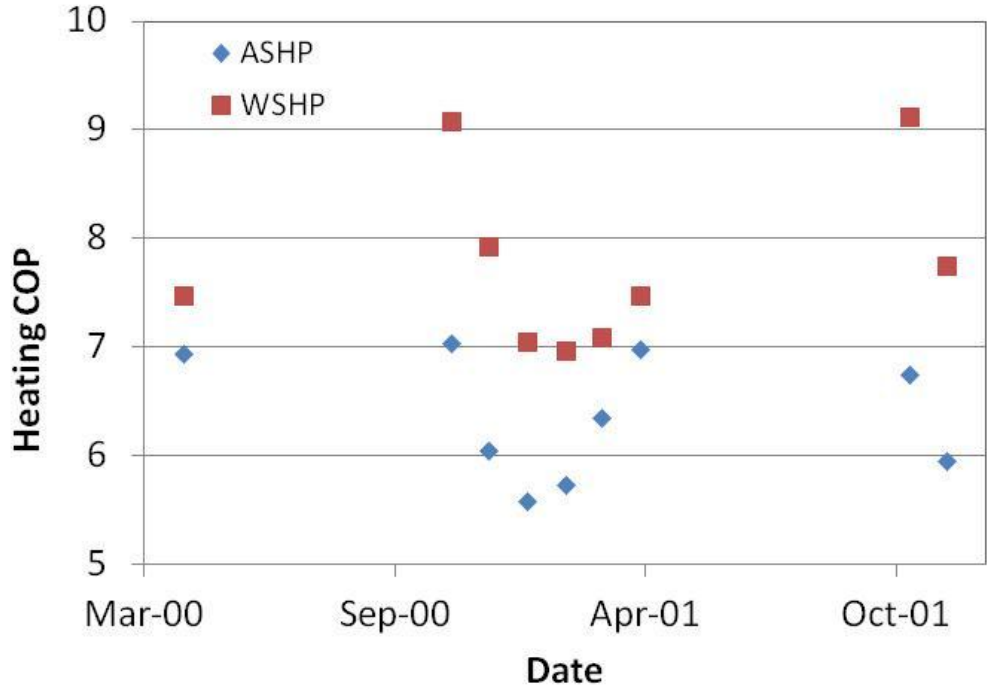

Figure 45: System heating COPs of ASHP and WSHP

4.4 Parametric study

As mentioned in the operation condition, seawater temperature change is fixed to 2K in the comparison study, and now the change in temperature is varied from 1K to 5K at a fixed water temperature of 17.5^{o}C and heating capacity is still fixed at 1 MW, and the change in evaporator capacity and COP are displayed in Figure 46.

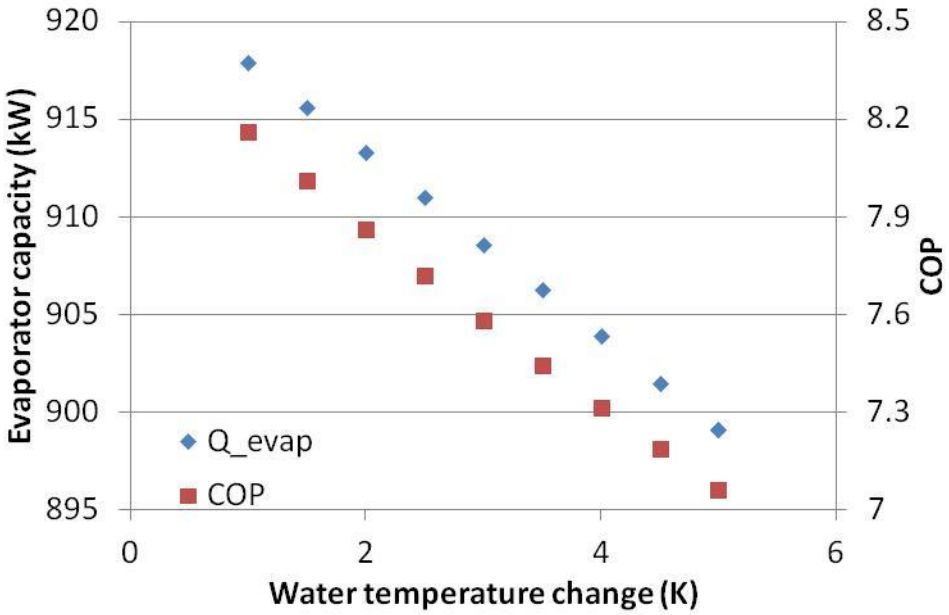

Figure 46: Evaporator capacity and COP vs. water temperature change

As indicated in Figure 46, when water temperature change gets larger, system COP and evaporator capacity both decrease. Even though increasing water temperature change can lower required water flow rate and water pump work, evaporation temperature also drops significantly due to the fixed 2.5K temperature difference between water outlet and evaporator inlet. Therefore, compressor work input becomes greater and system COP becomes lower, as explained in Figure 47.

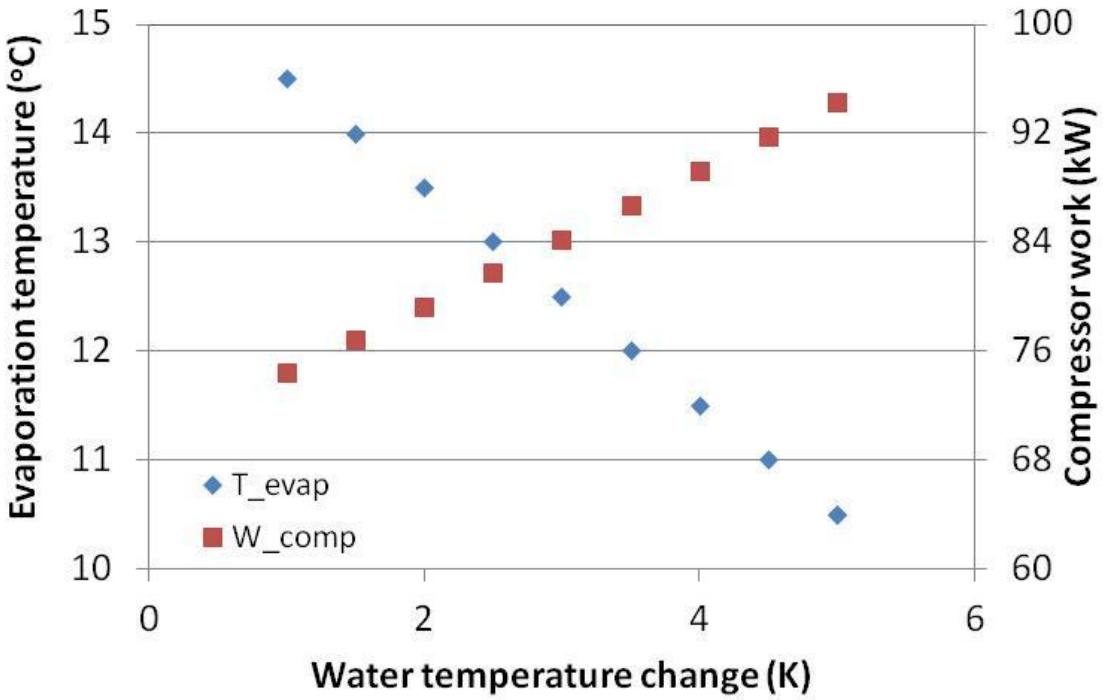

Figure 47: Evaporation temperature and compressor work vs. water temperature change

Due to a drop in evaporation temperature with increasing water temperature change, pressure ratio inside the compressor also increases, leading to a lower compressor efficiency and higher work input, which eventually lowers the overall COP.

4.5 Conclusions

Throughout the heating season in the simulation, WSHP has an average COP of 7.77, while ASHP only shows average COP of 6.37. In terms of system efficiency, WSHP clearly has an advantage over ASHP, especially when water like seawater shows better thermal profile than ambient air for most of the time. Also, parameters such allowable seawater temperature change has a large impact on the system performance, and they should be optimized to achieve highest system efficiency and maximum energy saving.

Nevertheless, when implementing WSHP, water quality is always a major concern, and the system must be able to handle all the possible issues related to water flow inside the evaporator.

Chapter 5. Conclusions

This study focuses on investigating the applicability of PHE for low temperature lift heat pump, specifically as an evaporator in the heat pump system, and water is the heat source. Due to the large water flow rate required by LTLHP, the evaporator was operated at low refrigerant mass flux, and such operating condition is different from works done other researchers. In order to provide unique evaporation heat transfer characteristics, I modified an existing test facility to better understand the behavior of PHE in LTLHP application. I first conducted water-to-water testing to calculate the water-side HTC, and I checked the energy balance to ensure the system had been well insulated. I measured two-phase evaporation heat transfer of refrigerant R134a inside a semi-welded PHE by varying refrigerant vapor quality, heat flux, evaporation pressure, and refrigerant mass flux. Based on the test results, heat flux had a positive effect on evaporation HTC, indicating the presence of nucleate boiling. However, a weak convective boiling was confirmed by the insignificant influence of vapor quality on evaporation HTC, but it was still present based on the slight effect of varying refrigerant mass flux. In addition, excess temperature also provided valuable insight into the evaporation mechanism, and it helped to explain the effect of evaporation pressure, which was different from observation made by other studies for nucleate boiling. After analyzing the two-phase heat transfer of R134a, I concluded that, due to small refrigerant mass flux, nucleate boiling was the more dominant mode, and convective boiling was still present.

Moreover, a simulation study was conducted to compare the heating performance of ASHP and WSHP, with the given temperature profile. Under the same operating

condition, COP of WSHP was significantly higher, thanks to a higher temperature of seawater than ambient air, resulting in reduced compressor work.

Chapter 6. Recommendations and Future Work

In this study, I investigated evaporation heat transfer of R134a inside a PHE, and the tested mass flux was much lower than the other existing studies done previously, as required by LTLHP applications. Due to the different testing conditions, a unique two-phase heat transfer characteristic of R134a was discovered. Likewise, this study was aimed specifically for low temperature lift heat pump applications, indicated by the low excess temperature observed.

Because of a limited pre-heating and post-heating capacity, mass flux of R134a through the PHE was constrained to a much lower range than existing studies done on PHE evaporation heat transfer. In order to cover a much wider mass flux range, pre-heating and post-heating capacity need to increase, and instead of using heating tapes, heat exchangers such as PHE could be substituted to significantly extend the mass flux range allowed. Plate geometry was not a parameter in this research study, and future test could include geometrical parameter such as chevron angle in the test matrix, and investigate the effect of chevron angle on HTC at low and high mass flux.

Furthermore, to better determine the applicability of PHE for low temperature lift heat pump system, as well as the energy saving from using WSHP over ASHP, a complete heat pump cycle should be constructed, including a compressor and an indoor condenser to provide heating. For the ASHP, a separate air to refrigerant evaporator is needed. The outdoor temperature and water temperature should be taken from actual temperature data for the whole heating season. Then under the same operating condition, WSHP with water pump and PHE as evaporator are compared with ASHP in terms of energy

consumption and overall system COP, and the advantage of WSHP over ASHP can be better justified. Also, because of facility limitation, only the evaporator was investigated in this study, and the test on condenser for LTLHP can be an extension of the current work. Finally, water fouling issue was not addressed in this study, and in practical applications, this remains as a very important factor to consider for WSHP. In the future projects, researchers should use waters with different quality, and investigate their impact on WSHP performance.

Reference

[1] Al-Jayyousi, O. R. Greywater reuse: towards sustainable water management. Desalination, 156 (2003), 181-192.

[2] Al-Marafie, A., Suri, R. K., Maheshwari, G. P. Choice of sink for air conditioning systems. International Journal of Refrigeration, 9 (1986), 34-38.

[3] ASHRAE handbook HVAC applications, SI edition. American Society of Heating, Refrigeration and Air-Conditioning Engineers, Inc., Atlanta, GA. 2011.

[4] Ayub, Z. H. Plate heat exchanger literature survey and new heat transfer and pressure drop correlation for refrigerant evaporators. Heat Transfer Engineering, 24 (2003), 3-16.

[5] Baek, N. C., Shin, U. C., Yoon, J. H. A study on the design and analysis of a heat pump heating system using wastewater as a heat source. Solar Energy, 78 (2005), 427-440.

[6] Buyukalaca, O. Ekinci, F. Yilmaz, T. Experimental investigation of Seyhan River and dam lake as heat source-sink for a heat pump. Energy, 28 (2003), 157-169.

[7] Cai, W. G., Wu, Y., Zhong, Y., Ren, H. China building energy consumption: Situation, challenges and corresponding measures. Energy Policy, 37 (2009), 2054-2059.

[8] Calm, J. M., Hourahan, G. C. "Refrigerant Data Summary," Engineered Systems, 18 (11): 74-88, November 2001.

[9] Calm, J. M., Domanski, p. R-22 replacement status. ASHRAE (2004), 46 (8), 29-39.

[10] Carpenter, N. E. Retrofitting HFC134a into existing CFC12 systems. International Journal of Refrigeration, 15 (1992), 332-339.

[11] Chen, D. A speech in one-year anniversary of Renewable Energy Law. State Development and Reform Commission; April 20, 2007.

[12] Chen, X., Zhang, G., Peng, J., Lin, X., Liu, T. The performance of an open-loop lake water heat pump system in south China. Applied Thermal Engineering, 26 (2006), 2255-2261.

[13] Chinese Statistic Yearbook 2002. National Bureau of Statistics, Beijing, China; 2002.

[14] The City of New York, Inventory of New York City greenhouse emissions, September 2010.

[15] Djordjevic, E. Kabelac, S. Flow boiling of R134a and ammonia in a plate heat exchanger. International Journal of Heat and Mass Transfer, 51 (2008), 6235-6242.

[16] Energy Information Administration, U.S. Department of Energy, 2011. Annual Energy Review 2011, Primary Energy Overview, Selected Years, 1949-2011.

[17] Energy Information Administration, U.S. Department of Energy, 2011. Annual Energy Review 2011, Primary Energy Production by Source, Selected Years, 1949-2011.

[18] Energy Information Administration, U.S. Department of Energy, 1993. Housing Characteristics 1993.

[19] Energy Information Administration, U.S. Department of Energy, 2005. 2005 Residential Energy Consumption Survey: Preliminary Housing Characteristics Tables.

[20] Energy Information Administration, International Energy Outlook 2006, U.S. Department of Energy, June 2006.

[21] Energy Information Administration, U.S. Department of Energy. State Energy Data 2010: Consumption. Table C1. Energy Consumption Overview: Estimates by Energy Source and End-Use Sector, 2010.

[22] Energy Star Program from the US Environmental Protection Agency.

Assessed http://www.energystar.gov.

[23] Faizal, M., Ahmed, M. R. Experimental studies on a corrugated plate heat exchanger for small temperature difference applications. Experimental Thermal and Fluid Science, 36 (2012), 242-248.

[24] Fernandes, C, S., Dias, R, P., Nobrega, J, M., Maia, J, M. Laminar flow in chevron-type plate heat exchangers: CFD analysis of tortuosity, shape factor and friction factor. Chemical Engineering and Processing, 46 (2007), 825-833.

[25] Fernandez-Seara, J., Uhia, F, J., Sieres, J., Campo, A. A general review of the Wilson plot method and its modifications to determine convection coefficients in heat exchange devices. Applied Thermal Engineering, 27 (2007), 2745-2757.

[26] Funamizu, N., Lida, M., Sakakura, Y., Takakuwa, T. Reuse of heat energy in wastewater: implementation examples in Japan. Water Science and Technology, 43 (2001), 277-285.

[27] Halimic, E., Ross, D., Agnew, B., Anderson, A., Potts, I. A comparison of the operating performance of alternative refrigerants. Applied Thermal Engineering, 23 (2003), 1441-1451.

[28] Han, D. H., Lee, K. J., Kim, Y. H. Experiments on the characteristics of evaporation of R410A in brazed plate heat exchangers with different geometric configurations. Applied Thermal Engineering, 23 (2003), 1209-1225.

[29] Han, X. H., Cui, L. Q., Chen, S. J., Chen, G. M., Wang, Q. A numerical and experimental study of chevron, corrugated plate heat exchangers. International Communications in Heat and Mass Transfer, 37 (2010), 1008-1014.

[30] Hsieh, Y.Y., Lin, T. F. Evaporation heat transfer and pressure drop of refrigerant R-410A flow in a vertical plate heat exchanger. Journal of Heat Transfer, 125 (2003), 852-857.

[31] Huang, J., Sheer, T, J., Bailey-McEwan, M. Heat transfer and pressure drop in plate heat exchanger refrigerant evaporators. International Journal of Refrigeration, 35 (2012), 325-335.

[32] Incropera, F. P., DeWitt, D. P. Fundamentals of Heat and Mass Transfer. Sixth Edition. New York: John Wiley & Sons; 2007 p. 620-640

[33] International Energy Agency (IEA), Key World Energy Statistics, 2006.

[34] Karagoz, S., Yilmaz, M., Comakli, O., Ozyurt, O. R134a and various mixtures of R22/R134a as an alternative to R22 in vapor compression heat pumps. Energy Conversion and Management, 45 (2004), 181-196.

[35] Khan, T. S., Khan, M. S., Chyu, M. C., Ayub, Z. H. Experimental investigation of evaporation heat transfer ad pressure drop of ammonia in a 60^{o} chevron plate heat exchanger. International Journal of Refrigeration, 35 (2012), 336-348.

[36] Khan, T. S., Khan, M. S., Chyu, M. C., Ayub, Z. H. Experimental investigation of single phase convective heat transfer coefficient in a corrugated plate heat exchanger for multiple plate configurations. Applied Thermal Engineering, 30 (2010), 1058-1065.

[37] Lee, H., Saleh, K., Hwang, Y., Radermacher, R. Optimization of novel heat exchanger design for the application to low temperature lift heat pump. Energy, 42 (2012), 204-212.

[38] Liu, L., Fu, L., Jiang, Y. Application of an exhaust heat recovery system for domestic hot water. Energy, 35 (2010), 1476-1481.

[39] Liu, S., Butler, D., Memon, F. A., Makropoulos, C., Avery, L., Jefferson, B. Impacts of residence time during storage on potential of water saving for grey water recycling system. Water Research, 44 (2010), 267-277.

[40] Longo, G, A. Heat transfer and pressure drop during HFC refrigerant saturated vapor condensation inside a brazed plate heat exchanger. International Journal of Heat and Mass Transfer, 53 (2010), 1079-1087.

[41] Ma, H., Oxley, L., Gibson, J., China's energy situation in the new millennium. Renewable and Sustainable Energy Reviews, 13 (2009), 1781-1799.

[42] Martin, H. A theoretical approach to predict the performance of chevron-type plate heat exchanger. Chemical Engineering and Processing, 35 (1996), 301-310.

[43] Meggers, F., Leibundgut, H. The potential of wastewater heat and exergy: Decentralized high-temperature recovery with a heat pump. Energy and Building, 43 (2011), 879-886.

[44] Murtishaw, S., Schipper, L. Disaggregated analysis of US energy consumption in the 1990s: evidence of the effects of the internet and rapid economic growth. Energy Policy, 29 (2001), 1335-1356.

[45] Nam, Y., Ooka, R., Shiba, Y. Development of dual-source hybrid heat pump system using groundwater and air. Energy and Buildings, 42 (2010), 909-916.

[46] Okamoto, S. A heat pump system with a latent heat storage utilizing seawater installed in an aquarium. Energy and Building, 38 (2006), 121-128.

[47] Omer, A. M. Ground-source heat pumps systems and applications. Renewable and Sustainable Energy Reviews, 12 (2008), 344-371.

[48] Paksoy, H. O., Gurbuz, Z., Turgut, B., Dikici, D., Evliya, H. Aquifer thermal storage (ATES) for air conditionings of a supermarket in Turkey. Renewable Energy, 29 (2004), 1991-1996.

[49] Perez-Lombard, L., Ortiz, J., Pout, C. A review on buildings energy consumption information. Energy and Buildings, 40 (2008), 394-398.

[50] Preisegger, E., Henrici, R. Refrigerant 134a: The first step into a new age of refrigerants. International Journal of Refrigeration, 15 (1992), 326-331.

[51] Schmid, F. Sewage water: interesting heat source for heat pumps and chillers. Proceedings of the 9th IEA Heat Pump Conference. 2008. Number 5.22

[52] Shen, C., Jiang, Y., Yao, Y., Deng, S. Experimental performance evaluation of a novel dry-expansion evaporator with defouling function in a wastewater source heat pump. Applied Energy, 95 (2012), 202-209.

[53] Song, Y. H., Akashi, Y., Yee, J. J. Effects of utilizing seawater as a cooling source system in a commercial complex. Energy and Building, 39 (2007), 1080-1087.

[54] Sun, Z., Gong, M., Li, Z., Wu, J. Nucleate pool boiling heat transfer coefficients of pure HFC 134a, HC290, HC600a and their binary and ternary mixtures. International Journal of Heat and Mass Transfer, 50 (2007), 94-104.

[55] SwissEnergy, 2005. ENERGIESCHWEIZ 2005. "Heizen und Kühlen mit Abwasser - Ratgeber für Bauherr-schaften und Gemeinden", Berne.

[56] Taboas, F., Valles, M., Bourouis, M., Coronas, A. Flow boiling heat transfer of ammonia/water mixture in a plate heat exchanger. International Journal of Refrigeration, 33 (2010), 695-705.

[57] Tassou, S. A. Heat recovery from sewage effluent using heat pumps. Heat Recovery System & CHP, Vol. 8, No.2 (1988), 141-148.

[58] Urchueguia, J.F., Zacares, M., Corberan, J. M., Montero, A., Martos, J., Witte, H. Comparison between the energy performance of a ground coupled water to water heat pump system and an air to water heat pump system for heating and cooling in typical conditions of the European Mediterranean coast. Energy Conversion and Management, 49 (2008), 2917-2923.

[59] Urkiaga, A., Fuentes, L., De, L., Bis, B., Chiru, E., Bodo, B., Hernandez, F., Wintgens, T. Methodologies for feasibility studies related to wastewater reclamation and reuse projects. Desalination, 187 (2006), 263-269.

[60] Wellsandt, S., Vamling, L. Heat transfer and pressure drop in a plate-type evaporator. International Journal of Refrigeration, 26 (2003), 180-188.

[61] Wu, Y. Chinese building energy conservation: existing situation, problems and policy, presentation on the International Conference on Sustainable Development in Building and Environment, Chongqing, China 24th – 27th 2003.

[62] Wyssen, I., Gasser, L., Kleingries, M., Wellig, B. High Efficient Heat Pumps For Small Temperature Lift Applications. 10th IEA Heat Pump Conference 2011, 16-19 May 2011, Tokyo, Japan.

[63] Yan, Y. Y., Lin, T. F. Evaporation heat transfer and pressure drop of refrigerant R-134a in a plate heat exchanger. Journal of Heat Transfer, 121 (1999), 118-127.

[64] Yang, H., Abbaspour, K. C. Analysis of wastewater reuse potential in Beijing. Desalination, 212 (2007), 238-250.

[65] Yang, W., Zhou, J., Xu, W., Zhang, G. Current status of ground-source heat pumps in China. Energy Policy, 38 (2010), 323-332.

[66] Yao, R., Li, B., Steemers, K. Energy policy and standard for built environment in China. Renewable Energy, 30 (2005), 1973-1988.

[67] Yik, F. W. H., Burnett, J., Prescott, I. Predicting air-conditioning energy consumption of a group of buildings using different heat rejection methods. Energy and Buildings, 33 (2001), 151-166.

[68] Yik, F. W. H., Burnett, J., Prescott, I. A study on the energy performance of three schemes for widening application of water-cooled air-conditioning systems in Hong Kong. Energy and Buildings, 33 (2001), 167-182.

[69] Zhang, P., Yang, Y., Shi, J., Zheng, Y., Wang, L., Li, X. Opportunities and challenges for renewable energy policy in China. Renewable and Sustainable Energy Reviews, 13 (2009), 439-449.

[70] Zhen, L., Lin, D. M., Shu, H. W., Jiang, S., Zhu, Y. X. District cooling and heating with seawater as heat source and sink in Dalian, China. Renewable Energy, 32 (2007), 2603-2616.

[71] Zhou, N., Lin, J. The reality and future scenarios of commercial building energy consumption in China. Energy and Buildings, 40 (2008), 2121-2127.

[72] Zhao, X. L., Fu, L., Zhang, S. G., Jiang, Y., Lai, Z. L. Study of the performance of an urban original source heat pump system. Energy Conversion and Management, 51 (2010), 765-770.